International Journal of Solids and Structures 304 (2024) 113015

Contents lists available at ScienceDirect

International Journal of Solids and Structures

journal homepage: www.elsevier.com/locate/ijsolstr

Dynamic multifield continualization of multilayered lattice-like metamaterials

Francesca Fantoni [a,*], Andrea Bacigalupo [b,*], Luigi Gambarotta [b]

[a] DICATAM, University of Brescia, Brescia, Italy
[b] DICCA, University of Genoa, Genoa, Italy

ARTICLE INFO

Keywords:
Beam lattice materials
Wave propagation
Frequency band structure
Enhanced continualization

ABSTRACT

This work focuses on dynamic continualization of multifield multilayered metamaterials in order to obtain energetically-consistent models able to provide an accurate description of the dispersive behavior of the corresponding discrete system. Continuum models, characterized by constitutive and inertial non-localities, have been identified through a recently proposed enhanced continualization scheme. They are identified by governing equations both of the integro-differential and higher-order gradient-type, whose regularization kernel or pseudo-differential functions accounting for shift operators are formally expanded in Taylor series. The adopted regularization kernel exhibits polar singularities at the edge of the first Brillouin zone, thus assuring the convergence of the frequency spectrum to the one of the Lagrangian system in the entire wave vector domain. The validity of the proposed approach is assessed through the investigation of multilayered discrete lattices with an antitetrachiral topology, where local resonators act as rigid links among the layers. The convergence of dispersion curves of the continuum model to the ones of the Lagrangian model is proved in the whole first Brillouin zone as the adopted continualization order increases, both considering the propagation and the spatial attenuation of Bloch waves inside the metamaterial. A low frequency continualization is also provided, leading to the identification of a first-order medium.

1. Introduction

Unique combinations of physical and mechanical properties, seldom observable in nature, can be obtained by micro-architected materials (Schaedler and Carter, 2016; Pham et al., 2019; Xia et al., 2019; Jia et al., 2019; Greer and Deshpande, 2019). Compared to fully dense solids, the introduction of new microstructures has allowed to expand the material property space in terms of, among others, strength, stiffness, and fracture toughness (Deshpande et al., 2001; Wadley et al., 2003; Romijn and Fleck, 2007; Fleck et al., 2010; Liu et al., 2012). The present work focuses on the dynamical *multifield* continualization of regular discrete media with lumped masses as the nodes, modeled as multilayered discrete periodic Lagrangian systems characterized by proper periodicity vectors. The term multifield refers to the presence of different displacement fields inside the periodic cell. It is known that scale effects arise from the periodic microstructure of these materials (Schraad and Triantafyllidis, 1997a,b; Aifantis and Willis, 2006; Bacigalupo and Gambarotta, 2021; Casolo, 2021), whereby processes at lower scales of observation influence the ones at higher scales and viceversa. Even if an accurate description of these lattice-like materials, representative of beam-lattice or block-lattice systems, can be achieved through discrete Lagrangian models (Colquitt et al., 2011; Vigliotti et al., 2014; Nannapaneni et al., 2021; Ostoja-Starzewski, 2002), the identification of continuum models can reveal extremely useful in capturing both the static and dynamic behavior of such periodic systems in a precise and, at the same time, concise way (Trovalusci and Masiani, 1999; Beex et al., 2014; Madeo et al., 2015; Bacigalupo and Gambarotta, 2017a), thus replacing the inhomogenities at lower scales by a continuum representation at higher scales. When a discrete system is identified with an homogeneous continuum the term continualization seems to be more appropriate than the term homogenization, which, instead, refers to the translation of an heterogeneous continuum into an equivalent homogeneous one (Rubin et al., 1995; Chang and Gao, 1995; Mühlhaus and Oka, 1996; Askes and Metrikine, 2005). A first-order continualization applied to a periodic discrete medium identifies the constitutive properties of the equivalent first-order (Cauchy) continuum, for which the standard stresses are algebraically related to the standard strains. Nevertheless, it is known from more than fifty years that the size effects arising from the underlying microstructure cannot be accurately captured by a classical local continuum (Mindlin, 1964) and, from this perspective, an enhanced continuum description

* Corresponding authors.
E-mail addresses: francesca.fantoni@unibs.it (F. Fantoni), andrea.bacigalupo@unige.it (A. Bacigalupo).

https://doi.org/10.1016/j.ijsolstr.2024.113015
Received 17 April 2024; Received in revised form 29 July 2024; Accepted 6 August 2024
Available online 21 August 2024

at a higher scale represents one of the possibilities to replace the heterogeneities at the lower scales. The inability of classical continuum theories to catch these size effects, which become increasingly relevant as the size of the component decreases, is due to the lack in the constitutive equations of an internal length, distinctive of the microstructure at hand (Forest and Sab, 1998). In a dynamic context, in order to accurately capture the physical phenomenon of wave dispersion occurring in discrete periodic materials, non-local continualization schemes can be adopted (Liu et al., 1999; Zhang et al., 2014; Challamel et al., 2015; Hache et al., 2017; Challamel et al., 2018), thus obtaining the so-called higher-order continua. Continuum governing equations can be determined from the minimization of a Lagrangian functional in which the kinetic and the potential energies are obtained in terms of a truncated Taylor series expansion of the continuum displacement field at the higher scale, this last adopted in order to approximate the displacement differences of adjacent nodes of the Lagrangian system. Nevertheless, it has been proved that such a continualization technique could lead to energetic inconsistencies for the continuum model, which results characterized by non positive defined potential energy density, although the discrete model is not affected by the same pathology (Bacigalupo and Gambarotta, 2017b; Kumar and McDowell, 2004; Rosenau, 2003). As a consequence, instabilities can arise in dynamics manifesting themselves by, among others, an unbounded growth of the response in time in the absence of external work, infinite group velocities in the short-wave limit, and the appearance of imaginary frequencies in the elastic field (Askes et al., 2002). The loss of ellipticity is also related to the loss of uniqueness in the static boundary value problem (Askes and Aifantis, 2011).

Alternatively, a continualization technique can directly operate on the discrete governing equations, where the continuous displacement field expanded in truncated series or the pseudo-differential operators expanded in truncated series are exploited in order to approximate the displacement differences among neighboring nodes in the discrete equations of motion (Bacigalupo and Gambarotta, 2017b; Askes and Metrikine, 2005; Askes et al., 2002). Pseudo-differential equations resulting from the use of shift operators can then be approximated by means of Padè approximants. This leads to the appearance of inertial non-localities in the governing equations of the equivalent non-local continuum, in the wake of non-local continua proposed by Mindlin (1964) that are characterized by constitutive and inertial characteristic lengths. Also in this case, though, the potential energy density can result non positive defined, thus causing the same issues described above.

A different continualization technique is based on the discrete Fourier transform or, equivalently, bilateral $\mathcal{Z}$-transform in space of the discrete governing equations, yielding to integro-differential equations of motion for the corresponding continuum model (Bacigalupo and Gambarotta, 2021, 2019; Andrianov et al., 2012; Charlotte and Truskinovsky, 2012; Kunin, 2012). If the integral kernels are expanded in power series or through a Padè approximant, higher-order differential equations are obtained for the continuum model, which, once again, could be characterized by inconsistencies from the energetic point of view. To overcome the problem, a so-called *enhanced* continualization procedure has been recently provided in Bacigalupo and Gambarotta (2019) for one-dimensional discrete models. The proposed continuum model reveals extremely accurate in approximating both the static and the dynamic response of the corresponding Lagrangian model. The continuum model is characterized by governing differential equations with both constitutive and inertial non-localities corresponding to a thermodynamic consistent Lagrangian functional. This last is obtained by means of the pseudo-differential equations defined at the macroscale formally expanded in power series, retrieving the shift operators concept.

In this work, the enhanced continualization technique proposed in Bacigalupo and Gambarotta (2021, 2019) is extended to multifield multilayered metamaterials with a complex topology. It is worth stressing that the presented high frequency continualization technique has been carried out in a completely general and rigorous mathematical framework that allows to capture the fundamental aspects of the physical problem at hand. Multifield continuum models can be identified by governing equations both of the integro-differential type and of the gradient-type, these lasts characterized by local or non-local inertial terms, depending on the choice made for the regularization kernel appearing in the down-scaling laws. In particular, the presence of inertial non-localities allows the identification of gradient-type multifield continuum models that are thermodynamically consistent. Dynamic instabilities in the short-wave limit are thus avoided, contrary to what happens, as previously mentioned, in the standard-like continualization obtained by means of a unitary regularization kernel, which is therefore analytic everywhere. The introduction of a proper regularization kernel showing polar singularities at the boundary of the first Brillouin zone in correspondence of the lattice coordination directions allows defining a convergence radius for its Taylor series approximation centered at the origin of the wave vector space. This guarantees the approximation of the frequency spectrum throughout the entire Brillouin zone, proving the convergence of the approximate spectrum to the actual one of the discrete lattice. The presented high frequency multifield continualization technique is amenable to be applied to discrete systems having any number of degrees of freedom. In the particular case of a monoatomic cell having three degrees of freedom in plane, the continualization scheme allows the identification of a non local generalized continuum of the integral type or of the gradient type, namely a generalized micropolar continuum. In the case of low approximation, a micropolar continuum with non local inertial terms can be identified, which results to be consistent from the thermodynamic point of view (Diana et al., 2023). By further imposing the symmetry of the stress tensor, the constitutive law can be condensed in order to obtain a local first-order continuum. In this work, a low frequency continualization scheme is also presented, leading to the identification of a first-order equivalent medium, whose frequency spectrum approximates the low frequency one of the discrete system in the long wavelength regime.

The work is organized as follows: in Section 2 the equations governing the dynamics of the discrete periodic Lagrangian systems are described. Particular attention is put on the derivation of the frequency spectrum of the lattice materials considering both homogeneous and non homogeneous waves, taking into account their propagation and spatial attenuation features. In the case of non homogeneous waves, the characteristic equation is an exponential polynomial in terms of the wave vector components. In Section 3 it is shown how the integral-type or gradient-type continuum model can be identified through the proposed dynamic high-frequency continualization technique. It is also shown how first-order models can be identified by employing spectral approximation techniques at low frequencies. An illustrative example is shown in Section 4, where the multifield continualization procedure is particularized for a single-layer lattice material with an antitetrachiral topology and for a bi-layered antitetrachiral discrete lattice having local resonators that serve as rigid links between the layers. Dispersive features of the discrete model are compared with the ones obtained through the continualization technique both in the standard-like case with unitary regularization kernel and in the enhanced case, confirming the validity of the proposed approach. It is also shown how the dispersion curves of the continuum model converge to the discrete ones by increasing the continualization order of the enhanced model. The performances of the low-frequency continualization are also investigated. Finally, the forced wave propagation is analyzed, demonstrating the capabilities of the continuum models to approximate the system response. Final remarks are reported in Section 5.

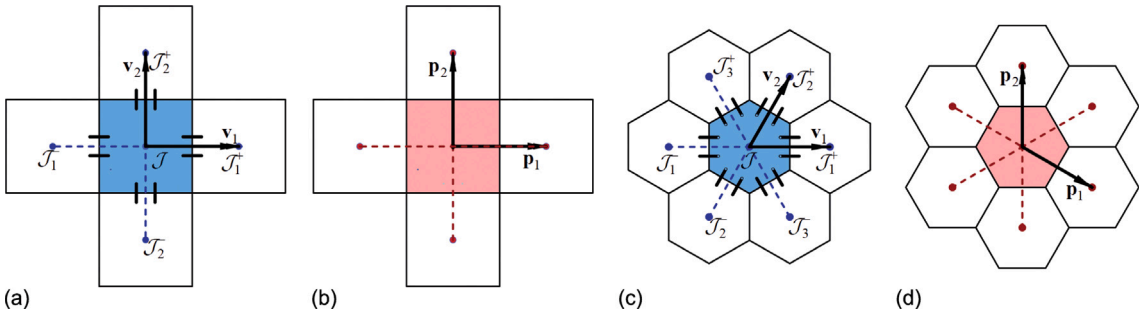

Fig. 1. Sketch of a generic lattice-like metamaterial containing in the periodic cell, highlighted in blue, a generic number of nodes with three degrees of freedom each. The periodic cell is connected to the adjacent ones by means of elastic links along the 2 or 3 coordination lines. In the physical space it is shown the lattice associated to the metamaterial characterized by two independent periodicity vectors $\mathbf{v}_1$ and $\mathbf{v}_2$ (figures (a) and (c)). In the wave vectors space it is shown the reciprocal lattice characterized by two independent periodicity vectors $\mathbf{p}_1$ and $\mathbf{p}_2$ and the corresponding periodic cell (not in scale), highlighted in red, or first Brillouin zone (figures (b) and (d)).

2. Dynamics of discrete periodic Lagrangian systems

One considers a two-dimensional periodic lattice-like material based on the spatial repetition of a cellular topology along $n/2$ lattice coordination lines, with n the lattice coordination number depending upon the specific planar topology under consideration (see Fig. 1). If the lattice-like material is representative of a beam-lattice system, one considers each periodic cell as characterized by a certain number of stiff rings with mass M_s and rotational inertia J_s, modeled as rigid bodies. Stiff rings are connected by light and flexible massless ligaments with length L, height w and unitary out-of-plane thickness, all modeled as unshearable Euler–Bernoulli beams with Young modulus E. A perfect rigid joint is assumed to exist between the rings and the beams. Each stiff ring is enhanced with a co-centered local resonator, which is a stiff disk with mass M_r and rotational inertia J_r, considered as a rigid body. Relative ring-resonator translational stiffness is denoted as k_d, while relative ring-resonator rotational one as k_θ. The set of Lagrangian coordinates for each periodic cell is constituted by vector $\mathbf{u}_{\mathcal{J}}^{(\ell)}(t)$, collecting the translational and rotational degrees of freedom for the stiff rings, and by vector $\mathbf{v}_{\mathcal{J}}^{(\ell)}(t)$ gathering the degrees of freedom of the resonators. Apex (ℓ) indicates that the cellular microstructure belongs to the ℓ-th layer, while subscript $\mathcal{J} = (i_1, \dots, i_{n/2})$ denotes that quantities are referred to the $\mathcal{J}$-th periodic cell. If $\mathbf{f}_{s_{\mathcal{J}}}^{(\ell)}(t)$ is the external force vector acting on the rings, and $\mathbf{f}_{r_{\mathcal{J}}}^{(\ell)}(t)$ the vector describing the interactions between the oscillators and the ℓ-th layer, the dynamics of the undamped lattice material is governed by the following system of ordinary differential equations

$$\begin{aligned}
&\mathbf{M}_s^{(\ell)}\,\ddot{\mathbf{u}}_{\mathcal{J}}^{(\ell)}(t) + \mathbf{K}_{ss}^{(\ell)}\,\mathbf{u}_{\mathcal{J}}^{(\ell)}(t) + \mathbf{K}_{sr}^{(\ell)}\,\mathbf{v}_{\mathcal{J}}^{(\ell)}(t)\\
&\quad + \sum_{\mathcal{P}_{[j]}}\left[\mathbf{K}_{ss_j}^{+(\ell)}\mathbf{u}_{\mathcal{J}_{[j]}^+}^{(\ell)}(t) + \mathbf{K}_{ss_j}^{-(\ell)}\mathbf{u}_{\mathcal{J}_{[j]}^-}^{(\ell)}(t)\right] = \mathbf{f}_{s_{\mathcal{J}}}^{(\ell)}(t),\\
&\mathbf{M}_r^{(\ell)}\,\ddot{\mathbf{v}}_{\mathcal{J}}^{(\ell)}(t) + \mathbf{K}_{rs}^{(\ell)}\,\mathbf{u}_{\mathcal{J}}^{(\ell)}(t) + \mathbf{K}_{rr}^{(\ell)}\,\mathbf{v}_{\mathcal{J}}^{(\ell)}(t) = \mathbf{f}_{r_{\mathcal{J}}}^{(\ell)}(t),
\end{aligned} \tag{1}$$

where $\mathcal{P}_{[j]} = \{j : j \in \mathbb{N}_{\geq 1}^{\leq n/2}\}$ gathers the j-values identifying the jth coordination line. This last is represented in the physical space by the vector $\mathbf{n}_j$. The sets $\mathcal{J}_{[j]}^{\pm} = (i_1, \dots, i_j \pm 1, \dots, i_{n/2})$, instead, identifies the adjacent cells along the jth coordination line, as depicted in Fig. 1. The components of mass matrices $\mathbf{M}_s^{(\ell)}$ and $\mathbf{M}_r^{(\ell)}$ and of the stiffness-like matrices $\mathbf{K}_{ss}^{(\ell)}$, $\mathbf{K}_{sr}^{(\ell)} = \mathbf{K}_{rs}^{(\ell)}$, $\mathbf{K}_{rr}$, $\mathbf{K}_{ss_j}^{+(\ell)}$ and $\mathbf{K}_{ss_j}^{-(\ell)}$ need to be detailed for the metamaterial topology at hand in terms of the geometrical and constitutive parameters.

Spatial periodicity of the lattice material makes it possible to efficiently investigate the propagation of elastic Bloch waves by applying a bilateral Laplace transform in time and a bilateral $\mathcal{Z}$-transform in space to the equations of motion (1). In this way, dispersion properties of the metamaterial can be studied in the frequency domain in terms of a continuous complex function of space. Bilateral Laplace transform of a real-valued function $q(t)$ is defined as $\mathcal{L}[q(t)] \doteq \int_{\mathbb{R}} q(t)\exp(-st)\mathrm{d}t = \hat{q}(s)$ with $\hat{q}(s) : \mathbb{C} \to \mathbb{C}$, while bilateral $\mathcal{Z}$-transform of function $q_{\mathcal{J}} : \mathbb{Z}^{n/2} \to \mathbb{C}$ is expressed as $\mathcal{Z}[q_{\mathcal{J}}] = \mathcal{Z}[q_{(i_1,\dots,i_{n/2})}] = \sum_{\mathcal{J}\in\mathbb{Z}^{n/2}} q_{(i_1,\dots,i_{n/2})} z_1^{-i_1}\dots z_{n/2}^{-i_{n/2}} = \check{q}(z_1, \dots, z_{n/2}) = \check{q}(\mathbf{z})$ with $\mathbf{z} = (z_1 \dots z_{n/2})^T \in \mathbb{C}^{n/2}$ and $\check{q}(\mathbf{z})$ a complex-valued function. Making use of the Laplace transform property $\mathcal{L}[\frac{\partial^n q(t)}{\partial t^n}] \doteq s^n\mathcal{L}[q(t)]$ and of the $\mathcal{Z}$-transform property $\mathcal{Z}[q_{(i_1\pm m_1,\dots,i_{n/2}\pm m_{n/2})}] \doteq z_1^{\pm m_1}\dots z_{n/2}^{\pm m_{n/2}}\mathcal{Z}[q_{(i_1,\dots,i_{n/2})}]$, Eqs. (1) are transformed into

$$\begin{aligned}
&s^2\,\mathbf{M}_s^{(\ell)}\hat{\mathring{\mathbf{u}}}^{(\ell)}(\mathbf{z},s) + \mathbf{K}_{ss}^{(\ell)}\,\hat{\mathring{\mathbf{u}}}^{(\ell)}(\mathbf{z},s) + \mathbf{K}_{sr}^{(\ell)}\,\hat{\mathring{\mathbf{v}}}^{(\ell)}(\mathbf{z},s)\\
&\quad + \sum_{\mathcal{P}_{[j]}}\left[\mathbf{K}_{ss_j}^{+(\ell)}z_j + \mathbf{K}_{ss_j}^{-(\ell)}z_j^{-1}\right]\hat{\mathring{\mathbf{u}}}^{(\ell)}(\mathbf{z},s) = \hat{\mathring{\mathbf{f}}}_s^{(\ell)}(\mathbf{z},s),\\
&s^2\,\mathbf{M}_r^{(\ell)}\hat{\mathring{\mathbf{v}}}^{(\ell)}(\mathbf{z},s) + \mathbf{K}_{rs}^{(\ell)}\,\hat{\mathring{\mathbf{u}}}^{(\ell)}(\mathbf{z},s) + \mathbf{K}_{rr}^{(\ell)}\,\hat{\mathring{\mathbf{v}}}^{(\ell)}(\mathbf{z},s) = \hat{\mathring{\mathbf{f}}}_r^{(\ell)}(\mathbf{z},s),
\end{aligned} \tag{2}$$

where symbol $\hat{\mathring{q}}(\mathbf{z},s) \doteq \mathcal{Z}[\hat{q}_{\mathcal{J}}(s)] = \mathcal{Z}[\mathcal{L}[q_{\mathcal{J}}(t)]]$ is used to denote the doubly-transformed quantity $q_{\mathcal{J}}(t)$. In the case of a multilayered structure, the resonators constitute a rigid joint between layers. In this sense, governing Eqs. (2) pertaining to each layer need to be combined through proper kinematic and dynamic relations. One supposes to have two different layers: a front one ($\ell = f$) and a back one ($\ell = b$). Inter-layer constraints in the transformed space read

$$\begin{aligned}
&\hat{\mathring{\mathbf{v}}}^{(f)}(\mathbf{z},s) = \hat{\mathring{\mathbf{v}}}^{(b)}(\mathbf{z},s) = \hat{\mathring{\mathbf{v}}}(\mathbf{z},s),\\
&\hat{\mathring{\mathbf{f}}}_r^{(f)}(\mathbf{z},s) = -\hat{\mathring{\mathbf{f}}}_r^{(b)}(\mathbf{z},s) = \hat{\mathring{\mathbf{f}}}_r(\mathbf{z},s).
\end{aligned} \tag{3}$$

After specifying system (2) for each layer and imposing constraints (3), simple algebraic manipulations lead to the following system

$$\begin{aligned}
&s^2\,\mathbf{M}_s^{(f)}\hat{\mathring{\mathbf{u}}}^{(f)}(\mathbf{z},s) + \mathbf{K}_{ss}^{(f)}\,\hat{\mathring{\mathbf{u}}}^{(f)}(\mathbf{z},s) + \mathbf{K}_{sr}^{(f)}\,\hat{\mathring{\mathbf{v}}}(\mathbf{z},s)\\
&\quad + \sum_{\mathcal{P}_{[j]}}\left[\mathbf{K}_{ss_j}^{+(f)}z_j + \mathbf{K}_{ss_j}^{-(f)}z_j^{-1}\right]\hat{\mathring{\mathbf{u}}}^{(f)}(\mathbf{z},s) = \hat{\mathring{\mathbf{f}}}_s^{(f)}(\mathbf{z},s),\\
&s^2\,\mathbf{M}_s^{(b)}\hat{\mathring{\mathbf{u}}}^{(b)}(\mathbf{z},s) + \mathbf{K}_{ss}^{(b)}\,\hat{\mathring{\mathbf{u}}}^{(b)}(\mathbf{z},s) + \mathbf{K}_{sr}^{(b)}\,\hat{\mathring{\mathbf{v}}}(\mathbf{z},s)\\
&\quad + \sum_{\mathcal{P}_{[j]}}\left[\mathbf{K}_{ss_j}^{+(b)}z_j + \mathbf{K}_{ss_j}^{-(b)}z_j^{-1}\right]\hat{\mathring{\mathbf{u}}}^{(b)}(\mathbf{z},s) = \hat{\mathring{\mathbf{f}}}_s^{(b)}(\mathbf{z},s),\\
&s^2\,\left(\mathbf{M}_r^{(f)} + \mathbf{M}_r^{(b)}\right)\hat{\mathring{\mathbf{v}}}(\mathbf{z},s) + \mathbf{K}_{rs}^{(f)}\,\hat{\mathring{\mathbf{u}}}^{(f)}(\mathbf{z},s) + \mathbf{K}_{rs}^{(b)}\,\hat{\mathring{\mathbf{u}}}^{(b)}(\mathbf{z},s)\\
&\quad + \left(\mathbf{K}_{rr}^{(f)} + \mathbf{K}_{rr}^{(b)}\right)\hat{\mathring{\mathbf{v}}}(\mathbf{z},s) = \mathbf{0}.
\end{aligned} \tag{4}$$

Imposing the quasi-periodicity Floquet–Bloch conditions is equivalent to mapping the complex variable z_j in the reciprocal $\mathbf{k}$-space through the relation $z_j = \exp(\imath\mathbf{x}_j \cdot \mathbf{k})$, with $\imath$ the imaginary unit, $\mathbf{x}_j = d_j\mathbf{n}_j$ the position vector of the reference cell centroid, d_j the characteristic size of the periodic cell along direction j, and $\mathbf{k} = k_i\mathbf{e}_i \in \mathbb{C}^2$ the complex wave vector written in terms of the plane canonical base $\{\mathbf{e}_1, \mathbf{e}_2\}$. Eqs. (4) can be concisely rephrased as

$$\mathbf{C}(\mathbf{k},s)\hat{\mathring{\mathbf{q}}}(\mathbf{k},s) = \hat{\mathring{\mathbf{f}}}(\mathbf{k},s), \tag{5}$$

with $\mathring{\mathbf{q}}(\mathbf{k},s)=\left(\mathring{\mathbf{u}}^{(f)}(\mathbf{k},s)\ \mathring{\mathbf{u}}^{(b)}(\mathbf{k},s)\ \mathring{\mathbf{v}}(\mathbf{k},s)\right)^T$, $\hat{\mathbf{f}}(\mathbf{k},s)=\left(\hat{\mathbf{f}}^{(f)}(\mathbf{k},s)\ \hat{\mathbf{f}}^{(b)}(\mathbf{k},s)\ \mathbf{0}\right)^T$ and

$$\mathbf{C}(\mathbf{k},s)=\begin{bmatrix} s^2\,\mathbf{M}_s^{(f)}+\mathbf{D}^{(f)}(\mathbf{k}) & \mathbf{0} & \mathbf{K}_{sr}^{(f)} \\ \mathbf{0} & s^2\,\mathbf{M}_s^{(b)}+\mathbf{D}^{(b)}(\mathbf{k}) & \mathbf{K}_{sr}^{(b)} \\ \mathbf{K}_{rs}^{(f)} & \mathbf{K}_{rs}^{(b)} & s^2\left(\mathbf{M}_r^{(f)}+\mathbf{M}_r^{(b)}\right)+\mathbf{K}_{rr}^{(f)}+\mathbf{K}_{rr}^{(b)} \end{bmatrix}, \tag{6}$$

where $\mathbf{D}^{(\ell)}(\mathbf{k})=\mathbf{K}_{ss}^{(\ell)}+\sum_{\mathcal{P}_{[j]}}\left[\mathbf{K}_{ss_j}^{+(\ell)}\exp(\imath\mathbf{x}_j\cdot\mathbf{k})+\mathbf{K}_{ss_j}^{-(\ell)}\exp(\imath\mathbf{x}_j\cdot\mathbf{k})^{-1}\right]$ with $\ell=f,b$. From the third of Eqs. (4) it is possible to express the vector $\mathring{\mathbf{v}}(\mathbf{k},s)$ collecting the degrees of freedom of the resonators in terms of the ones of the lattices $\mathring{\mathbf{u}}^{(\ell)}(\mathbf{k},s)$. In this way, the system (4) can be condensed into the form

$$\begin{aligned}&\left[s^2\mathbf{M}_s^{(f)}-\mathbf{K}_{sr}^{(f)}\mathbf{B}^{-1}(s)\mathbf{K}_{rs}^{(f)}+\mathbf{D}^{(f)}(\mathbf{k})\right]\mathring{\mathbf{u}}^{(f)}(\mathbf{k},s)-\left[\mathbf{K}_{sr}^{(f)}\mathbf{B}^{-1}(s)\mathbf{K}_{rs}^{(b)}\right]\mathring{\mathbf{u}}^{(b)}(\mathbf{k},s)\\&\quad=\hat{\mathbf{f}}_s^{(f)}(\mathbf{k},s),\\&\left[s^2\mathbf{M}_s^{(b)}-\mathbf{K}_{sr}^{(b)}\mathbf{B}^{-1}(s)\mathbf{K}_{rs}^{(b)}+\mathbf{D}^{(b)}(\mathbf{k})\right]\mathring{\mathbf{u}}^{(b)}(\mathbf{k},s)-\left[\mathbf{K}_{sr}^{(b)}\mathbf{B}^{-1}(s)\mathbf{K}_{rs}^{(f)}\right]\mathring{\mathbf{u}}^{(f)}(\mathbf{k},s)\\&\quad=\hat{\mathbf{f}}_s^{(b)}(\mathbf{k},s)\end{aligned} \tag{7}$$

with

$$\mathbf{B}(s)=s^2\left(\mathbf{M}_r^{(f)}+\mathbf{M}_r^{(b)}\right)+\mathbf{K}_{rr}^{(f)}+\mathbf{K}_{rr}^{(b)}. \tag{8}$$

The nonnull components of the matrix $\mathbf{B}^{-1}(s)=\mathrm{adj}\,(\mathbf{B})/\det[\mathbf{B}]$, with symbol adj$(\cdot)$ denoting the adjugate of a matrix, are characterized by poles at infinity in correspondence of the zeros of the denominator (if they do not overlap to the zeros of the numerator) associated to the presence of the resonators. Such frequencies, as shown in the following, approximate the central frequencies of the band gaps which appear in the frequency spectrum of the metamaterial.

In order to investigate the propagation and the spatial attenuation of Bloch waves inside the metamaterial, one imposes that $s=\imath\omega$, with $\omega\in\mathbb{R}$ the circular frequency, and the wave vector $\mathbf{k}$ is expressed in terms of its real and imaginary components $\mathbf{k}_R\in\mathbb{R}^2$ and $\mathbf{k}_I\in\mathbb{R}^2$ as $\mathbf{k}=\mathbf{k}_R+\imath\mathbf{k}_I=\left(k_{1_R}+\imath k_{1_I}\right)\mathbf{e}_1+\left(k_{2_R}+\imath k_{2_I}\right)\mathbf{e}_2$. The real component $\mathbf{k}_R$ is directed perpendicularly to planes of constant phase, while imaginary component $\mathbf{k}_I$ is normal to planes with constant amplitude, thus allowing the definition of two unit vectors

$$\mathbf{n}_R=\frac{\mathbf{k}_R}{\|\mathbf{k}_R\|_2}=\cos\theta_R\mathbf{e}_1+\sin\theta_R\mathbf{e}_2,\qquad \mathbf{n}_I=\frac{\mathbf{k}_I}{\|\mathbf{k}_I\|_2}=\cos\theta_I\mathbf{e}_1+\sin\theta_I\mathbf{e}_2, \tag{9}$$

which represent the direction of propagation and spatial attenuation, respectively, of the Bloch wave. Furthermore, real and imaginary cartesian components of the wave vector can be explicited in terms of θ_R and θ_I as $k_{1_R}=k_R\,\mathbf{n}_R\cdot\mathbf{e}_1=k_R\cos\theta_R$, $k_{2_R}=k_R\,\mathbf{n}_R\cdot\mathbf{e}_2=k_R\sin\theta_R$, $k_{1_I}=k_I\,\mathbf{n}_I\cdot\mathbf{e}_1=k_I\cos\theta_I$ and $k_{2_I}=k_I\,\mathbf{n}_I\cdot\mathbf{e}_2=k_I\sin\theta_I$. When $\mathbf{n}_R\neq\mathbf{n}_I$ the wave is denoted as non homogeneous and the matrix $\mathbf{C}(\mathbf{k},\omega)$ of Eq. (6) is an exponential polynomial in $\mathbf{k}$ with matricial coefficients. As a consequence of this, the associated characteristic equation $\det[\mathbf{C}(\mathbf{k},\omega)]=0$ is an exponential polynomial in $\mathbf{k}$. Denoting with $\mathcal{P}(\mathbf{k},\omega)=\det[\mathbf{C}(\mathbf{k},\omega)]=\mathcal{P}_R(\mathbf{k},\omega)+\imath\,\mathcal{P}_I(\mathbf{k},\omega)$ the complex characteristic polynomial, the metamaterial frequency spectrum is obtained from the intersection of two hypersurfaces immersed in $\mathbb{R}^5$, derived by imposing the vanishing of the real and imaginary parts of $\mathcal{P}$, namely

$$\begin{cases}\mathcal{P}_R(k_R,k_I,\theta_R,\theta_I,\omega)=0\\ \mathcal{P}_I(k_R,k_I,\theta_R,\theta_I,\omega)=0\end{cases} \tag{10}$$

In particular, if directions of propagation and attenuation are fixed, namely θ_R and θ_I are known, the frequency spectrum is obtained through the intersection of two surfaces immersed in $\mathbb{R}^3$. In Appendix A it is shown how the matrix $\mathbf{D}^{(\ell)}(\mathbf{k})$ can be expressed in terms of the Floquet multipliers and, consequently, how Eq. (5) for the free propagation case becomes a polynomial eigenproblem in the complex Floquet multipliers with, in general, non integer exponents. When the propagation direction $\mathbf{n}_R$ coincides with the attenuation one $\mathbf{n}_I$, namely $\mathbf{n}_R=\mathbf{n}_I=\mathbf{n}$, or $\theta_R=\theta_I=\theta$, the wave is denoted as homogeneous and the wave vector can be written as $\mathbf{k}=\left(k_R+\imath k_I\right)\mathbf{n}=k\,\mathbf{n}\in\mathbb{C}^2$, with k the complex wave number. In this case, the complex characteristic polynomial is $\mathcal{P}(k,\mathbf{n},\omega)$ and the frequency spectrum is obtained, once again, through the intersection of two hypersurfaces immersed in $\mathbb{R}^5$ showing difficulties analogous to the ones previously described for the non homogeneous waves. Once again, in Appendix A it is shown how, once the matrix $\mathbf{D}^{(\ell)}(\mathbf{k})$ is expressed in terms of a single Floquet multiplier, it results in an exponential polynomial with non integer exponents unless the propagation direction $\mathbf{n}$ coincides with one of the reciprocal lattice's periodicity directions.

Finally, in the simpler case in which only the propagation of the Bloch wave is investigated, the wave vector $\mathbf{k}$ is such that $\mathbf{k}\in\mathbb{R}^2$, and, since $s=\imath\omega$, Eq. (5) under the free propagation condition, becomes a quadratic eigenproblem parameterized in $\mathbf{k}$, where ω is the eigenvalue, namely

$$\left(\mathbf{K}(\mathbf{k})-\omega^2\mathbf{M}\right)\mathring{\mathbf{q}}(\mathbf{k},\omega^2)=\mathbf{0}, \tag{11}$$

with

$$\mathbf{K}(\mathbf{k})=\begin{bmatrix}\mathbf{D}^{(f)}(\mathbf{k}) & \mathbf{0} & \mathbf{K}_{sr}^{(f)}\\ \mathbf{0} & \mathbf{D}^{(b)} & \mathbf{K}_{sr}^{(b)}\\ \mathbf{K}_{rs}^{(f)} & \mathbf{K}_{rs}^{(b)} & \mathbf{K}_{rr}^{(f)}+\mathbf{K}_{rr}^{(b)}\end{bmatrix},\qquad \mathbf{M}=\begin{bmatrix}\mathbf{M}_s^{(f)} & \mathbf{0} & \mathbf{0}\\ \mathbf{0} & \mathbf{M}_s^{(b)} & \mathbf{0}\\ \mathbf{0} & \mathbf{0} & \mathbf{M}_r^{(f)}+\mathbf{M}_r^{(b)}\end{bmatrix}. \tag{12}$$

Analogously to what was previously done, expressing the degrees of freedom of the resonators in terms of the ones of the lattices, the system (11) can be condensed and characterized by a matrix whose components show singularities in correspondence of the resonators natural frequencies.

It is worth noting that the procedure detailed in the present Section to investigate the dispersion properties of the metamaterial can be particularized and simplified for the case of a discrete lattice constituted by a single layer without resonators. In this case, in fact, the Eqs. (1) describing the dynamics of the system reduce to

$$\mathbf{M}_s\ \ddot{\mathbf{u}}_{\mathcal{J}}(t)+\mathbf{K}_{ss}\,\mathbf{u}_{\mathcal{J}}(t)+\sum_{\mathcal{P}_{[j]}}\left[\mathbf{K}_{ss_j}^{+}\,\mathbf{u}_{\mathcal{J}_{[j]}^{+}}(t)+\mathbf{K}_{ss_j}^{-}\,\mathbf{u}_{\mathcal{J}_{[j]}^{-}}(t)\right]=\mathbf{f}_{s_{\mathcal{J}}}(t), \tag{13}$$

and, after the application of a bilateral Laplace transform in time and a bilateral $\mathcal{Z}$-transform in space, with $z_j=\exp(\imath\,\mathbf{x}_j\cdot\mathbf{k})$, spectral properties of the Lagrangian system can be studied in the $(\mathbf{k},s)$-space from the resolution of the following eigenproblem

$$\left[s^2\,\mathbf{M}_s+\mathbf{D}(\mathbf{k})\right]\mathring{\mathbf{u}}(\mathbf{k},s)=\mathbf{0} \tag{14}$$

with

$$\mathbf{D}(\mathbf{k})=\mathbf{K}_{ss}+\sum_{\mathcal{P}_{[j]}}\left[\mathbf{K}_{ss_j}^{+}\exp(\imath\mathbf{x}_j\cdot\mathbf{k})+\mathbf{K}_{ss_j}^{-}\exp(\imath\mathbf{x}_j\cdot\mathbf{k})^{-1}\right].$$

All the considerations previously made for non homogeneous and homogeneous waves are obviously still valid for this simpler case.

3. Continualization schemes

In the following, Section 3.1 is dedicated to the presentation of the dynamic high frequency continualization technique. It leads to continuum models characterized by integral-type or higher-order gradient-type governing equations. The low frequency continualization procedure is successively described in Section 3.2, this last providing the identification of a first-order continuum.

3.1. High frequency continualization

One defines the continuous field $\tilde{\mathbf{q}}(\mathbf{k},t)=\left(\tilde{\mathbf{u}}^{(f)}(\mathbf{k},t)\ \tilde{\mathbf{u}}^{(b)}(\mathbf{k},t)\ \tilde{\mathbf{v}}(\mathbf{k},t)\right)^T$ through the following definition

$$\tilde{\mathbf{q}}(\mathbf{k},t)=\mathcal{F}\left[\mathbf{q}(\mathbf{x},t)\right]\doteq\mathcal{Z}\left[\mathbf{q}_{\mathcal{J}}(t)\right]\Big|_{z_j=\exp(\imath\mathbf{x}_j\cdot\mathbf{k})}, \tag{15}$$

where $\mathcal{F}$ is the space Fourier transform with complex argument, defined for a generic vector function $\mathbf{y}(\mathbf{x},t)$ as $\mathcal{F}[\mathbf{y}(\mathbf{x},t)] = \int_{\mathbb{R}^2} \mathbf{y}(\mathbf{x},t)\exp(-\imath\mathbf{k}\cdot\mathbf{x})\,\mathrm{d}\mathbf{x} \doteq \tilde{\mathbf{y}}(\mathbf{k},t)$. The introduction of the $\mathbf{k}$-dependent regularization kernel $F^{-1}(\mathbf{k})$, defined as

$$F^{-1}(\mathbf{k}) \doteq \prod_{\mathcal{P}_{[j]}} \frac{\exp(\imath\mathbf{x}_j\cdot\mathbf{k}) - \exp(-\imath\mathbf{x}_j\cdot\mathbf{k})}{2\imath\mathbf{x}_j\cdot\mathbf{k}} = \prod_{\mathcal{P}_{[j]}} \frac{\sinh(\imath\mathbf{x}_j\cdot\mathbf{k})}{\imath\mathbf{x}_j\cdot\mathbf{k}}$$
$$= \prod_{\mathcal{P}_{[j]}} \frac{\sin(\mathbf{x}_j\cdot\mathbf{k})}{\mathbf{x}_j\cdot\mathbf{k}} = \prod_{\mathcal{P}_{[j]}} \mathrm{sinc}(\mathbf{x}_j\cdot\mathbf{k}) \tag{16}$$

allows defining the non-local upscaling relation in the $\mathbf{k}$-space

$$\tilde{\mathbf{q}}^R(\mathbf{k},t) \doteq F^{-1}(\mathbf{k})\tilde{\mathbf{q}}(\mathbf{k},t) = F^{-1}(\mathbf{k})\mathcal{Z}\left[\mathbf{q}_{\mathcal{J}}(t)\right]\Big|_{z_j=\exp(\imath\mathbf{x}_j\cdot\mathbf{k})}. \tag{17}$$

The regularization kernel (16) is the one characterizing the enhanced continualization procedure (see Fig. 2), which differs from the standard-like continualization scheme for which the regularization kernel is unitary. Using the inverse Fourier transform with complex argument $\mathcal{F}^{-1}[\tilde{\mathbf{y}}(\mathbf{k},t)] = \frac{1}{(2\pi i)^2}\int_{\mathbb{C}^2_\zeta} \tilde{\mathbf{y}}(\mathbf{k},t)\exp(\imath\mathbf{k}\cdot\mathbf{x})\mathrm{d}\mathbf{k} \doteq \mathbf{y}(\mathbf{x},t)$ where subgroup $\mathbb{C}^2_\zeta = \left\{\mathbf{k} = k_j\mathbf{e}_j \,:\, k_j \in \lim_{\rho_j\to\infty}\left(\zeta_j - \imath\rho_j;\zeta_j+\imath\rho_j\right)\right\}$, with ζ_j a suitably selected real constant within the domain of holomorphy of function $\tilde{\mathbf{y}}(\mathbf{k},t)$, the field $\tilde{\mathbf{q}}^R(\mathbf{k},t)$ can be transformed into a continuous field of physical space and time as

$$\mathbf{q}^R(\mathbf{x},t) = \mathcal{F}^{-1}\left[F^{-1}(\mathbf{k})\tilde{\mathbf{q}}(\mathbf{k},t)\right] = \mathcal{F}^{-1}\left[F^{-1}(\mathbf{k})\right] * \mathcal{F}^{-1}\left[\tilde{\mathbf{q}}(\mathbf{k},t)\right]$$
$$= \mathcal{F}^{-1}\left[F^{-1}(\mathbf{k})\right] * \mathbf{q}(\mathbf{x},t), \tag{18}$$

where symbol $*$ denotes the convolution product with respect to the spatial variable. If the inverse Fourier transform of the kernel $F^{-1}(\mathbf{k})$ is made explicit, the regularized continuous field $\mathbf{q}^R(\mathbf{x},t)$ becomes

$$\mathbf{q}^R(\mathbf{x},t) = \frac{\pi}{2}\int_{\mathbb{R}^2}\prod_{n=1}^{2}\mathrm{rect}\left(\frac{x_n-\xi_n}{2}\right)\mathbf{q}(\xi,t)d\xi$$
$$= \frac{\pi}{2}\int_{\mathcal{A}}\prod_{n=1}^{2}\mathrm{rect}\left(\frac{x_n-\xi_n}{2}\right)\mathbf{q}(\xi,t)d\xi, \tag{19}$$

with $\mathcal{A}$ denoting the periodic cell in the continuum model and rect$(\bullet)$ the rectangular function with compact support of size $\mathcal{A}$.[1] By means of definition (15), system (4) becomes

$$\mathbf{M}_s^{(\ell)}\ddot{\tilde{\mathbf{u}}}^{(\ell)}(\mathbf{k},t) + \mathbf{K}_{sr}^{(\ell)}\tilde{\mathbf{v}}(\mathbf{k},t) + \mathbf{D}^{(\ell)}(\mathbf{k})\tilde{\mathbf{u}}^{(\ell)}(\mathbf{k},t) = \tilde{\mathbf{f}}_s^{(\ell)}(\mathbf{k},t),$$
$$\left(\mathbf{M}_r^{(f)} + \mathbf{M}_r^{(b)}\right)\ddot{\tilde{\mathbf{v}}}(\mathbf{k},t) + \mathbf{K}_{rs}^{(f)}\tilde{\mathbf{u}}^{(f)}(\mathbf{k},t) + \mathbf{K}_{rs}^{(b)}\tilde{\mathbf{u}}^{(b)}(\mathbf{k},t)$$
$$+ \left(\mathbf{K}_{rr}^{(f)} + \mathbf{K}_{rr}^{(b)}\right)\tilde{\mathbf{v}}(\mathbf{k},t) = \mathbf{0}. \tag{21}$$

where $\ell = f,b$ and $\tilde{\mathbf{f}}_s^{(\ell)}(\mathbf{k},t)$ is the Fourier transform of the corresponding continuous field in $\mathbf{x}$ and t. Through (17), system (21) can be written as a set of ordinary differential equations in $\tilde{\mathbf{q}}^R(\mathbf{k},t)$. It reads

$$\mathbf{M}_s^{(\ell)}F(\mathbf{k})\ddot{\tilde{\mathbf{u}}}^{(\ell)R}(\mathbf{k},t) + \mathbf{K}_{sr}^{(\ell)}F(\mathbf{k})\tilde{\mathbf{v}}^R(\mathbf{k},t)$$
$$+ \mathbf{D}^{(\ell)}(\mathbf{k})F(\mathbf{k})\tilde{\mathbf{u}}^{(\ell)R}(\mathbf{k},t) = \tilde{\mathbf{f}}_s^{(\ell)}(\mathbf{k},t),$$
$$\left(\mathbf{M}_r^{(f)} + \mathbf{M}_r^{(b)}\right)F(\mathbf{k})\ddot{\tilde{\mathbf{v}}}^R(\mathbf{k},t) + \mathbf{K}_{rs}^{(f)}F(\mathbf{k})\tilde{\mathbf{u}}^{(f)R}(\mathbf{k},t) + \mathbf{K}_{rs}^{(b)}F(\mathbf{k})\tilde{\mathbf{u}}^{(b)R}(\mathbf{k},t) +$$
$$+ \left(\mathbf{K}_{rr}^{(f)} + \mathbf{K}_{rr}^{(b)}\right)F(\mathbf{k})\tilde{\mathbf{v}}^R(\mathbf{k},t) = \mathbf{0}. \tag{22}$$

The set of integro-differential equations governing the dynamics of the system in the physical $\mathbf{x}$-space and time is finally obtained by an inverse Fourier transform of (22), namely

$$\mathcal{F}^{-1}\left[\mathbf{M}_s^{(\ell)}F(\mathbf{k})\mathcal{F}\left[\ddot{\mathbf{u}}^{(\ell)R}(\mathbf{x},t)\right]\right.$$
$$\left. + \mathbf{K}_{sr}^{(\ell)}F(\mathbf{k})\mathcal{F}\left[\mathbf{v}^R(\mathbf{x},t)\right] + \mathbf{D}^{(\ell)}(\mathbf{k})F(\mathbf{k})\mathcal{F}\left[\mathbf{u}^{(\ell)R}(\mathbf{x},t)\right]\right] = \mathcal{F}^{-1}\left[\tilde{\mathbf{f}}_s^{(\ell)}(\mathbf{k},t)\right],$$
$$\mathcal{F}^{-1}\left[\left(\mathbf{M}_r^{(f)} + \mathbf{M}_r^{(b)}\right)F(\mathbf{k})\mathcal{F}[\ddot{\mathbf{v}}^R(\mathbf{x},t)] + \mathbf{K}_{rs}^{(f)}F(\mathbf{k})\mathcal{F}\left[\mathbf{u}^{(f)R}(\mathbf{x},t)\right]\right.$$
$$+ \mathbf{K}_{rs}^{(b)}F(\mathbf{k})\mathcal{F}\left[\mathbf{u}^{(b)R}(\mathbf{x},t)\right] +$$
$$\left. + \left(\mathbf{K}_{rr}^{(f)} + \mathbf{K}_{rr}^{(b)}\right)F(\mathbf{k})\mathcal{F}\left[\mathbf{v}^R(\mathbf{x},t)\right]\right] = \mathbf{0}. \tag{23}$$

It is worth noting that $\mathbf{k}$-dependent terms in (23) are actually dependent on variable $\imath\mathbf{k}$ and hence, they can be renamed as $F(\mathbf{k}) = F_\Delta(\imath\mathbf{k})$, $\mathbf{D}^{(\ell)}(\mathbf{k}) = \mathbf{D}_\Delta^{(\ell)}(\imath\mathbf{k})$. Following Hörmander (2007), Kohn (1973), Bacigalupo and Gambarotta (2019), it is possible to define the following pseudo-differential operators uniquely

$$\mathcal{F}^{-1}\left[\mathbf{M}_s^{(\ell)}F_\Delta(\imath\mathbf{k})\mathcal{F}\left[\ddot{\mathbf{u}}^{(\ell)R}(\mathbf{x},t)\right]\right] \doteq \mathbf{M}_s^{(\ell)}F_\Delta\left[D_1,D_2\right]\ddot{\mathbf{u}}^{(\ell)R}(\mathbf{x},t),$$
$$\mathcal{F}^{-1}\left[\mathbf{K}_{sr}^{(\ell)}F_\Delta(\imath\mathbf{k})\mathcal{F}\left[\mathbf{v}^R(\mathbf{x},t)\right]\right] \doteq \mathbf{K}_{sr}^{(\ell)}F_\Delta\left[D_1,D_2\right]\mathbf{v}^R(\mathbf{x},t),$$
$$\mathcal{F}^{-1}\left[\mathbf{D}_\Delta^{(\ell)}(\imath\mathbf{k})F_\Delta(\imath\mathbf{k})\mathcal{F}\left[\mathbf{u}^{(\ell)R}(\mathbf{x},t)\right]\right] \doteq \mathbf{D}_\Delta^{(\ell)}\left[D_1,D_2\right]F_\Delta\left[D_1,D_2\right]\mathbf{u}^{(\ell)R}(\mathbf{x},t),$$
$$\mathcal{F}^{-1}\left[\left(\mathbf{M}_r^{(f)} + \mathbf{M}_r^{(b)}\right)F_\Delta(\imath\mathbf{k})\mathcal{F}[\ddot{\mathbf{v}}^R(\mathbf{x},t)]\right] \doteq \left(\mathbf{M}_r^{(f)} + \mathbf{M}_r^{(b)}\right)F_\Delta\left[D_1,D_2\right]\ddot{\mathbf{v}}^R(\mathbf{x},t),$$
$$\mathcal{F}^{-1}\left[\mathbf{K}_{rs}^{(f)}F_\Delta(\imath\mathbf{k})\mathcal{F}\left[\mathbf{u}^{(f)R}(\mathbf{x},t)\right]\right] \doteq \mathbf{K}_{rs}^{(f)}F_\Delta\left[D_1,D_2\right]\mathbf{u}^{(f)R}(\mathbf{x},t),$$
$$\mathcal{F}^{-1}\left[\mathbf{K}_{rs}^{(b)}F_\Delta(\imath\mathbf{k})\mathcal{F}\left[\mathbf{u}^{(b)R}(\mathbf{x},t)\right]\right] \doteq \mathbf{K}_{rs}^{(b)}F_\Delta\left[D_1,D_2\right]\mathbf{u}^{(b)R}(\mathbf{x},t),$$
$$\mathcal{F}^{-1}\left[\left(\mathbf{K}_{rr}^{(f)} + \mathbf{K}_{rr}^{(b)}\right)F_\Delta(\imath\mathbf{k})\mathcal{F}\left[\mathbf{v}^R(\mathbf{x},t)\right]\right] \doteq \left(\mathbf{K}_{rr}^{(f)} + \mathbf{K}_{rr}^{(b)}\right)F_\Delta\left[D1,D2\right]\mathbf{v}^R(\mathbf{x},t), \tag{24}$$

where $D_k\mathbf{y}(\mathbf{x},t) = \partial\mathbf{y}(\mathbf{x},t)/\partial x_k$, with $\mathbf{y}(\mathbf{x},t)$ a generic vector-valued continuous field of $\mathbf{x}$ and t and $k = 1,2$. The pseudo-differential operator $F_\Delta(D_1,D_2)$ is plotted in terms of the pseudo-variables D_1 and D_2 in Fig. 2. In the light of definition (24), the system (23) can equivalently be written as

$$\mathbf{M}_s^{(\ell)}F_\Delta\left[D_1,D_2\right]\ddot{\mathbf{u}}^{(\ell)R}(\mathbf{x},t) + \mathbf{K}_{sr}^{(\ell)}F_\Delta\left[D_1,D_2\right]\mathbf{v}^R(\mathbf{x},t)$$
$$+ \mathbf{D}_\Delta^{(\ell)}\left[D_1,D_2\right]F_\Delta\left[D_1,D_2\right]\mathbf{u}^{(\ell)R}(\mathbf{x},t) = \mathbf{f}_s^{(\ell)}(\mathbf{x},t),$$
$$\left(\mathbf{M}_r^{(f)} + \mathbf{M}_r^{(b)}\right)F_\Delta\left[D_1,D_2\right]\ddot{\mathbf{v}}^R(\mathbf{x},t) + \mathbf{K}_{rs}^{(f)}F_\Delta\left[D_1,D_2\right]\mathbf{u}^{(f)R}(\mathbf{x},t)$$
$$+ \mathbf{K}_{rs}^{(b)}F_\Delta\left[D_1,D_2\right]\mathbf{u}^{(b)R}(\mathbf{x},t) +$$
$$+ \left(\mathbf{K}_{rr}^{(f)} + \mathbf{K}_{rr}^{(b)}\right)F_\Delta\left[D_1,D_2\right]\mathbf{v}^R(\mathbf{x},t) = \mathbf{0}. \tag{25}$$

The integral-type non-local continuum field Eqs. (23), or, equivalently, their pseudo-differential form (25), once transformed in the $(\mathbf{k},s)$-space by means of a Fourier transform with complex argument in space and a bilateral Laplace transform in time, define a frequency band structure that is identical to the one of the corresponding discrete lattice material. The spectrum identity follows from definition (15) and it subsists within the regularization kernel's domain of holomorphy.

In order to obtain the field equations of generalized gradient-type higher-order continuum models, the $\mathbf{k}$-dependent integral kernels appearing in the equations system (22) can be formally expanded in Taylor series as

$$F(\mathbf{k}) \backsim \sum_{r\in\mathbb{N}}\sum_{|\alpha|=r}\frac{1}{r!}\begin{pmatrix} r \\ p_1+p_2\end{pmatrix}F_{,\alpha}\big|_{\mathbf{k}=\mathbf{0}}\mathbf{k}^\alpha =$$
$$= \sum_{r\in\mathbb{N}}\sum_{|\alpha|=r}\frac{1}{p_1!p_2!}\left.\frac{\partial^{|\alpha|}F}{\partial k_{\alpha_1}\partial k_{\alpha_2}\ldots\partial k_{\alpha_r}}\right|_{\mathbf{k}=\mathbf{0}}k_{\alpha_1}k_{\alpha_2}\ldots k_{\alpha_r}$$
$$= \sum_{p_1,p_2\in\mathbb{N}}\frac{1}{p_1!p_2!}\left.\frac{\partial^{p_1+p_2}F}{\partial k_1^{p_1}\partial k_2^{p_2}}\right|_{\mathbf{k}=\mathbf{0}}k_1^{p_1}k_2^{p_2},$$
$$\mathbf{D}^{(\ell)}(\mathbf{k})F(\mathbf{k}) \backsim \sum_{r\in\mathbb{N}}\sum_{|\alpha|=r}\frac{1}{r!}\begin{pmatrix} r \\ p_1+p_2\end{pmatrix}(\mathbf{D}^{(\ell)}F)_{,\alpha}\big|_{\mathbf{k}=\mathbf{0}}\mathbf{k}^\alpha =$$

[1] In the framework of pseudo-differential operators, as introduced in formula (24), it is worth stressing that from the inverse Fourier transform of the mapping (17) and taking into account the definition (15) in the physical space, the relation between the directional derivative of the regularized continuum field and the effective nodal displacement in the discrete model is given in the form

$$\left(\prod_{\mathcal{P}_{[j]}}\mathbf{n}_j\cdot\mathbf{D}\,\mathbf{q}^R(\mathbf{x},t)\right)\Big|_{\mathbf{x}_{\mathcal{J}}} \doteq \prod_{\mathcal{P}_{[j]}}\frac{\exp(d_j\mathbf{n}_j\cdot\mathbf{D}) - \exp(-d_j\mathbf{n}_j\cdot\mathbf{D})}{2d_j}\mathbf{q}_{\mathcal{J}}(t), \tag{20}$$

with $\mathbf{n}_j$ the unit vector identifying the jth coordination line, $\mathbf{D} = [D_1\ D_2]^T$, and $\mathbf{x}_0$ the position of the generic reference cell centroid. The term $\exp(d_j\mathbf{n}_j\cdot\mathbf{D})$ plays the role of a shift operator according to Jordán (1965) and Rota (1964). In the one-dimensional case, Eq. (20) becomes the definition of the first derivative obtained using the finite difference method with a second-order accuracy. In the two-dimensional case it has a similar meaning in the sense that the product of the directional first derivatives of the macrofield along the lattice coordination lines is set equal to the product of the associated directional first derivatives of the discrete field described as a finite difference with a second order accuracy.

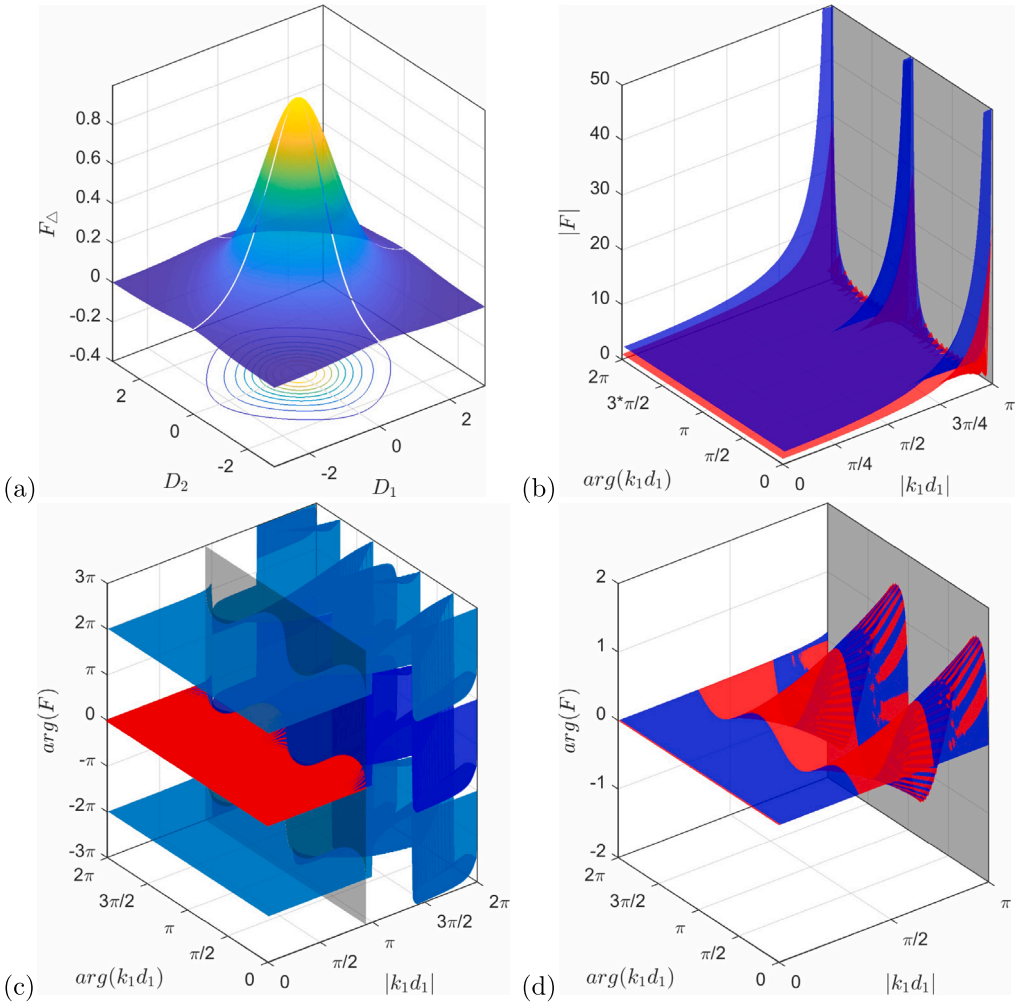

Fig. 2. (a) $F_\triangle$ in terms of D_1 and D_2. (b) Magnitude of F vs $|k_1 d_1|$ and $\arg(k_1 d_1)$ (blue) and its Taylor series expansion of order $r = 64$ (red). (c) Argument of F vs $|k_1 d_1|$ and $\arg(k_1 d_1)$ (blue) and its Taylor series expansion of order $r = 64$ (red). (d) Zoom of the argument of F vs $|k_1 d_1|$ and $\arg(k_1 d_1)$ (blue) and its Taylor series expansion of order $r = 64$ (red).

$$= \sum_{r\in\mathbb{N}} \sum_{|\alpha|=r} \frac{1}{p_1!p_2!} \left.\frac{\partial^{|\alpha|}\mathbf{D}^{(\ell)}F}{\partial k_{\alpha_1}\partial k_{\alpha_2}\ldots\partial k_{\alpha_r}}\right|_{\mathbf{k}=\mathbf{0}} k_{\alpha_1}k_{\alpha_2}\ldots k_{\alpha_r}$$

$$= \sum_{p_1,p_2\in\mathbb{N}} \frac{1}{p_1!p_2!} \left.\frac{\partial^{p_1+p_2}\mathbf{D}^{(\ell)}F}{\partial k_1^{p_1}\partial k_2^{p_2}}\right|_{\mathbf{k}=\mathbf{0}} k_1^{p_1}k_2^{p_2}, \tag{26}$$

where α is a multi-index of length $|\alpha| = r$ and such that $\alpha_1, \alpha_2, \ldots, \alpha_r = 1, 2$, while p_1 and p_2 are integer numbers which measure the repetitions of k_1 and k_2 occurring in the differential operator of order $|\alpha| = p_1 + p_2 = r$ and $\binom{r}{p_1+p_2}$ is the multinomial coefficient. Since $(\imath\,\mathbf{k})^\alpha = \imath^{|\alpha|}\mathbf{k}^\alpha = \imath^r k_1^{p_1}k_2^{p_2}$, the system (22) becomes

$$\sum_{p_1,p_2\in\mathbb{N}} \frac{1}{\imath^r p_1!p_2!}\left(\imath^r k_1^{p_1}k_2^{p_2}\right)\left\{\mathbf{M}_s^{(\ell)} \left.\frac{\partial^r F}{\partial k_1^{p_1}\partial k_2^{p_2}}\right|_{\mathbf{k}=\mathbf{0}} \ddot{\tilde{\mathbf{u}}}^{(\ell)R}(\mathbf{k},t)\right.$$
$$+ \mathbf{K}_{sr}^{(\ell)} \left.\frac{\partial^r F}{\partial k_1^{p_1}\partial k_2^{p_2}}\right|_{\mathbf{k}=\mathbf{0}} \tilde{\mathbf{v}}^R(\mathbf{k},t) +$$
$$\left. + \left.\frac{\partial^r \mathbf{D}^{(\ell)}F}{\partial k_1^{p_1}\partial k_2^{p_2}}\right|_{\mathbf{k}=\mathbf{0}} \tilde{\mathbf{u}}^{(\ell)R}(\mathbf{k},t)\right\} = \tilde{\mathbf{f}}_s^{(\ell)}(\mathbf{k},t),$$

$$\sum_{p_1,p_2\in\mathbb{N}} \frac{1}{\imath^r p_1!p_2!}\left(\imath^r k_1^{p_1}k_2^{p_2}\right)\left\{\left(\mathbf{M}_r^{(f)} + \mathbf{M}_r^{(b)}\right) \left.\frac{\partial^r F}{\partial k_1^{p_1}\partial k_2^{p_2}}\right|_{\mathbf{k}=\mathbf{0}} \ddot{\tilde{\mathbf{v}}}^R(\mathbf{k},t)\right.$$
$$+ \mathbf{K}_{rs}^{(f)} \left.\frac{\partial^r F}{\partial k_1^{p_1}\partial k_2^{p_2}}\right|_{\mathbf{k}=\mathbf{0}} \tilde{\mathbf{u}}^{(f)R}(\mathbf{k},t) +$$
$$+ \mathbf{K}_{rs}^{(b)} \left.\frac{\partial^r F}{\partial k_1^{p_1}\partial k_2^{p_2}}\right|_{\mathbf{k}=\mathbf{0}} \tilde{\mathbf{u}}^{(b)R}(\mathbf{k},t)$$
$$\left. + \left(\mathbf{K}_{rr}^{(f)} + \mathbf{K}_{rr}^{(b)}\right) \left.\frac{\partial^r F}{\partial k_1^{p_1}\partial k_2^{p_2}}\right|_{\mathbf{k}=\mathbf{0}} \tilde{\mathbf{v}}^R(\mathbf{k},t)\right\} = \mathbf{0}. \tag{27}$$

Recalling the inverse Fourier transform property

$$\mathcal{F}^{-1}\left[(\imath^r k_1^{p_1}k_2^{p_2})\mathcal{F}\left[\mathbf{y}^R(\mathbf{x},t)\right]\right] = \mathcal{F}^{-1}\left[(\imath^r k_1^{p_1}k_2^{p_2})\bar{\mathbf{y}}^R(\mathbf{k},t)\right] = \frac{\partial^r \mathbf{y}^R(\mathbf{x},t)}{\partial x_1^{p_1}\partial x_2^{p_2}} \tag{28}$$

the system (27), after some simple manipulations, can be written in the $(\mathbf{x},t)$-space as

$$\sum_{p_1,p_2\in\mathbb{N}} \frac{1}{\imath^{r+2}p_1!p_2!}\left\{\mathbf{K}_{sr}^{(\ell)} \left.\frac{\partial^r F}{\partial k_1^{p_1}\partial k_2^{p_2}}\right|_{\mathbf{k}=\mathbf{0}} \frac{\partial^r \mathbf{v}^R(\mathbf{x},t)}{\partial x_1^{p_1}\partial x_2^{p_2}}\right.$$
$$\left. + \left.\frac{\partial^r \mathbf{D}^{(\ell)}F}{\partial k_1^{p_1}\partial k_2^{p_2}}\right|_{\mathbf{k}=\mathbf{0}} \frac{\partial^r \mathbf{u}^{(\ell)R}(\mathbf{x},t)}{\partial x_1^{p_1}\partial x_2^{p_2}}\right\} +$$
$$+ \mathbf{f}_s^{(\ell)}(\mathbf{x},t) = \mathbf{M}_s^{(\ell)} \sum_{p_1,p_2\in\mathbb{N}} \frac{1}{\imath^r p_1!p_2!} \left.\frac{\partial^r F}{\partial k_1^{p_1}\partial k_2^{p_2}}\right|_{\mathbf{k}=\mathbf{0}} \frac{\partial^r \ddot{\mathbf{u}}^{(\ell)R}(\mathbf{x},t)}{\partial x_1^{p_1}\partial x_2^{p_2}},$$
$$\sum_{p_1,p_2\in\mathbb{N}} \frac{1}{\imath^{r+2}p_1!p_2!}\left\{\mathbf{K}_{rs}^{(f)} \left.\frac{\partial^r F}{\partial k_1^{p_1}\partial k_2^{p_2}}\right|_{\mathbf{k}=\mathbf{0}} \frac{\partial^r \mathbf{u}^{(f)R}(\mathbf{x},t)}{\partial x_1^{p_1}\partial x_2^{p_2}}\right.$$
$$\left. + \mathbf{K}_{rs}^{(b)} \left.\frac{\partial^r F}{\partial k_1^{p_1}\partial k_2^{p_2}}\right|_{\mathbf{k}=\mathbf{0}} \frac{\partial^r \mathbf{u}^{(b)R}(\mathbf{x},t)}{\partial x_1^{p_1}\partial x_2^{p_2}} +\right.$$

$$+\left(\mathbf{K}_{rr}^{(f)}+\mathbf{K}_{rr}^{(b)}\right)\left.\frac{\partial^r F}{\partial k_1^{p_1}\partial k_2^{p_2}}\right|_{\mathbf{k}=\mathbf{0}}\left.\frac{\partial^r \mathbf{v}^R(\mathbf{x},t)}{\partial x_1^{p_1}\partial x_2^{p_2}}\right\}$$
$$=\left(\mathbf{M}_{r}^{(f)}+\mathbf{M}_{r}^{(b)}\right)\sum_{p_1,p_2\in\mathbb{N}}\frac{1}{\imath^r p_1!p_2!}\left.\frac{\partial^r F}{\partial k_1^{p_1}\partial k_2^{p_2}}\right|_{\mathbf{k}=\mathbf{0}}\left.\frac{\partial^r \ddot{\mathbf{v}}^R(\mathbf{x},t)}{\partial x_1^{p_1}\partial x_2^{p_2}}\right. . \tag{29}$$

Eqs. (29) represent the infinite-order field equations of a gradient-type continuum model expressed in the $(\mathbf{x},t)$-space and, because of definition (15), they are characterized by the same frequency spectrum of the corresponding Lagrangian system. This happens, once again, within the domain of holomorphy of the integral kernel $F(\mathbf{k})$. It is worth observing that the obtained field equations for the gradient-type continuum model are characterized by both constitutive and inertial non-localities, these last disappearing in the case of a standard-like continualization with a unitary regularization kernel. In order to obtain the differential field equations of a continuum model of order N, the Taylor series expansions (26) need to be truncated at the order $r=2N$, which is denoted as continualization order. System (29) thus becomes

$$\sum_{r=0}^{2N}\sum_{p_1+p_2=r}\frac{1}{\imath^{r+2}p_1!p_2!}\left\{\mathbf{K}_{sr}^{(\ell)}\left.\frac{\partial^r F}{\partial k_1^{p_1}\partial k_2^{p_2}}\right|_{\mathbf{k}=\mathbf{0}}\frac{\partial^r \mathbf{v}^R(\mathbf{x},t)}{\partial x_1^{p_1}\partial x_2^{p_2}}\right.$$
$$+\left.\frac{\partial^r \mathbf{D}^{(\ell)}F}{\partial k_1^{p_1}\partial k_2^{p_2}}\right|_{\mathbf{k}=\mathbf{0}}\left.\frac{\partial^r \mathbf{u}^{(\ell)R}(\mathbf{x},t)}{\partial x_1^{p_1}\partial x_2^{p_2}}\right\}+$$
$$+\mathbf{f}_s^{(\ell)}(\mathbf{x},t)=\mathbf{M}_s^{(\ell)}\sum_{r=0}^{2N}\sum_{p_1+p_2=r}\frac{1}{\imath^r p_1!p_2!}\left.\frac{\partial^r F}{\partial k_1^{p_1}\partial k_2^{p_2}}\right|_{\mathbf{k}=\mathbf{0}}\left.\frac{\partial^r \ddot{\mathbf{u}}^{(\ell)R}(\mathbf{x},t)}{\partial x_1^{p_1}\partial x_2^{p_2}}\right.,$$
$$\sum_{r=0}^{2N}\sum_{p_1+p_2=r}\frac{1}{\imath^{r+2}p_1!p_2!}\left\{\mathbf{K}_{rs}^{(f)}\left.\frac{\partial^r F}{\partial k_1^{p_1}\partial k_2^{p_2}}\right|_{\mathbf{k}=\mathbf{0}}\left.\frac{\partial^r \mathbf{u}^{(f)R}(\mathbf{x},t)}{\partial x_1^{p_1}\partial x_2^{p_2}}\right.\right.$$
$$+\left.\mathbf{K}_{rs}^{(b)}\left.\frac{\partial^r F}{\partial k_1^{p_1}\partial k_2^{p_2}}\right|_{\mathbf{k}=\mathbf{0}}\left.\frac{\partial^r \mathbf{u}^{(b)R}(\mathbf{x},t)}{\partial x_1^{p_1}\partial x_2^{p_2}}\right.+\right.$$
$$+\left.\left(\mathbf{K}_{rr}^{(f)}+\mathbf{K}_{rr}^{(b)}\right)\left.\frac{\partial^r F}{\partial k_1^{p_1}\partial k_2^{p_2}}\right|_{\mathbf{k}=\mathbf{0}}\left.\frac{\partial^r \mathbf{v}^R(\mathbf{x},t)}{\partial x_1^{p_1}\partial x_2^{p_2}}\right\}\right.$$
$$=\left(\mathbf{M}_{r}^{(f)}+\mathbf{M}_{r}^{(b)}\right)\sum_{r=0}^{2N}\sum_{p_1+p_2=r}\frac{1}{\imath^r p_1!p_2!}\left.\frac{\partial^r F}{\partial k_1^{p_1}\partial k_2^{p_2}}\right|_{\mathbf{k}=\mathbf{0}}\cdot$$
$$\cdot\left.\frac{\partial^r \ddot{\mathbf{v}}^R(\mathbf{x},t)}{\partial x_1^{p_1}\partial x_2^{p_2}}\right. . \tag{30}$$

By means of a Fourier transform in space with complex argument and a Laplace transform in time, Eqs. (30) are written in the $(\mathbf{k},s)$-space as

$$\sum_{r=0}^{2N}\sum_{p_1+p_2=r}\frac{1}{p_1!p_2!}k_1^{p_1}k_2^{p_2}\left\{\mathbf{K}_{sr}^{(\ell)}\left.\frac{\partial^r F}{\partial k_1^{p_1}\partial k_2^{p_2}}\right|_{\mathbf{k}=\mathbf{0}}\mathring{\mathbf{v}}^R(\mathbf{k},s)\right.$$
$$+\left.\frac{\partial^r \mathbf{D}^{(\ell)}F}{\partial k_1^{p_1}\partial k_2^{p_2}}\right|_{\mathbf{k}=\mathbf{0}}\mathring{\mathbf{u}}^{(\ell)R}(\mathbf{k},s)+$$
$$+\left.\mathbf{M}_s^{(\ell)}\left.\frac{\partial^r F}{\partial k_1^{p_1}\partial k_2^{p_2}}\right|_{\mathbf{k}=\mathbf{0}}s^2\mathring{\mathbf{u}}^{(\ell)R}(\mathbf{k},s)\right\}=\mathring{\mathbf{f}}_s^{(\ell)}(\mathbf{k},s),$$
$$\sum_{r=0}^{2N}\sum_{p_1+p_2=r}\frac{1}{p_1!p_2!}k_1^{p_1}k_2^{p_2}\left\{\mathbf{K}_{rs}^{(f)}\left.\frac{\partial^r F}{\partial k_1^{p_1}\partial k_2^{p_2}}\right|_{\mathbf{k}=\mathbf{0}}\mathring{\mathbf{u}}^{(f)R}(\mathbf{k},s)\right.$$
$$+\left.\mathbf{K}_{rs}^{(b)}\left.\frac{\partial^r F}{\partial k_1^{p_1}\partial k_2^{p_2}}\right|_{\mathbf{k}=\mathbf{0}}\mathring{\mathbf{u}}^{(b)R}(\mathbf{k},s)+\right.$$
$$+\left.\left(\mathbf{K}_{rr}^{(f)}+\mathbf{K}_{rr}^{(b)}\right)\left.\frac{\partial^r F}{\partial k_1^{p_1}\partial k_2^{p_2}}\right|_{\mathbf{k}=\mathbf{0}}\mathring{\mathbf{v}}^R(\mathbf{k},s)\right.$$
$$+\left.\left(\mathbf{M}_{r}^{(f)}+\mathbf{M}_{r}^{(b)}\right)\left.\frac{\partial^r F}{\partial k_1^{p_1}\partial k_2^{p_2}}\right|_{\mathbf{k}=\mathbf{0}}s^2\mathring{\mathbf{v}}^R(\mathbf{k},s)\right\}=\mathbf{0}, \tag{31}$$

which allows the investigation of the spectral response of the N-order gradient-type continuum model. Analogously to what is done in the discrete case, the equations system (31) can be briefly written as

$$\mathbf{C}^h(\mathbf{k},s)\mathring{\mathbf{q}}^R(\mathbf{k},s)=\mathring{\mathbf{f}}(\mathbf{k},s), \tag{32}$$

with $\mathring{\mathbf{q}}^R(\mathbf{k},s)=\left(\mathring{\mathbf{u}}^{(f)R}(\mathbf{k},s)\,\mathring{\mathbf{u}}^{(b)R}(\mathbf{k},s)\,\mathring{\mathbf{v}}^R(\mathbf{k},s)\right)^T$ and $\mathring{\mathbf{f}}(\mathbf{k},s)=\left(\mathring{\mathbf{f}}^{(f)}(\mathbf{k},s)\right.$ $\left.\mathring{\mathbf{f}}^{(b)}(\mathbf{k},s)\,\mathbf{0}\right)^T$. The matrix $\mathbf{C}^h(\mathbf{k},s)$ reads

$$\mathbf{C}^h(\mathbf{k},s)=\begin{bmatrix}\mathbf{C}^h_{\mathbf{u}^{(f)}\mathbf{u}^{(f)}}(\mathbf{k},s) & \mathbf{0} & \mathbf{C}^h_{\mathbf{u}^{(f)}\mathbf{v}}(\mathbf{k})\\ \mathbf{0} & \mathbf{C}^h_{\mathbf{u}^{(b)}\mathbf{u}^{(b)}}(\mathbf{k},s) & \mathbf{C}^h_{\mathbf{u}^{(b)}\mathbf{v}}(\mathbf{k})\\ \mathbf{C}^h_{\mathbf{v}\mathbf{u}^{(f)}}(\mathbf{k}) & \mathbf{C}^h_{\mathbf{v}\mathbf{u}^{(b)}}(\mathbf{k}) & \mathbf{C}^h_{\mathbf{v}\mathbf{v}}(\mathbf{k},s)\end{bmatrix} \tag{33}$$

with

$$\mathbf{C}^h_{\mathbf{u}^{(\ell)}\mathbf{u}^{(\ell)}}(\mathbf{k},s)=\sum_{r=0}^{2N}\sum_{p_1+p_2=r}\frac{1}{p_1!p_2!}k_1^{p_1}k_2^{p_2}\left(\left.\frac{\partial^r F}{\partial k_1^{p_1}\partial k_2^{p_2}}\right|_{\mathbf{k}=\mathbf{0}}s^2\mathbf{M}_s^{(\ell)}\right.$$
$$+\left.\left.\frac{\partial^r \mathbf{D}^{(\ell)}F}{\partial k_1^{p_1}\partial k_2^{p_2}}\right|_{\mathbf{k}=\mathbf{0}}\right),$$
$$\mathbf{C}^h_{\mathbf{u}^{(\ell)}\mathbf{v}}(\mathbf{k})=\sum_{r=0}^{2N}\sum_{p_1+p_2=r}\frac{1}{p_1!p_2!}k_1^{p_1}k_2^{p_2}\left.\frac{\partial^r F}{\partial k_1^{p_1}\partial k_2^{p_2}}\right|_{\mathbf{k}=\mathbf{0}}\mathbf{K}_{sr}^{(\ell)},$$
$$\mathbf{C}^h_{\mathbf{v}\mathbf{u}^{(\ell)}}(\mathbf{k})=\sum_{r=0}^{2N}\sum_{p_1+p_2=r}\frac{1}{p_1!p_2!}k_1^{p_1}k_2^{p_2}\left.\frac{\partial^r F}{\partial k_1^{p_1}\partial k_2^{p_2}}\right|_{\mathbf{k}=\mathbf{0}}\mathbf{K}_{rs}^{(\ell)},$$
$$\mathbf{C}^h_{\mathbf{v}\mathbf{v}}(\mathbf{k},s)=\sum_{r=0}^{2N}\sum_{p_1+p_2=r}\frac{1}{p_1!p_2!}k_1^{p_1}k_2^{p_2}\left.\frac{\partial^r F}{\partial k_1^{p_1}\partial k_2^{p_2}}\right|_{\mathbf{k}=\mathbf{0}}$$
$$\times\left[s^2\left(\mathbf{M}_r^{(f)}+\mathbf{M}_r^{(b)}\right)+\left(\mathbf{K}_{rr}^{(f)}+\mathbf{K}_{rr}^{(b)}\right)\right]. \tag{34}$$

and $\ell=f,b$. Also for the continuum model at hand, the system (32) can be condensed since $\mathring{\mathbf{v}}^R(\mathbf{k},s)$ results

$$\mathring{\mathbf{v}}^R(\mathbf{k},s)=-\left(\mathbf{C}^h_{\mathbf{v}\mathbf{v}}(\mathbf{k},s)\right)^{-1}\left[\mathbf{C}^h_{\mathbf{v}\mathbf{u}^{(\mathbf{f})}}(\mathbf{k})\mathring{\mathbf{u}}^{(f)}(\mathbf{k},s)+\mathbf{C}^h_{\mathbf{v}\mathbf{u}^{(\mathbf{b})}}(\mathbf{k})\mathring{\mathbf{u}}^{(b)}(\mathbf{k},s)\right]. \tag{35}$$

The system (32) thus becomes

$$\left[\mathbf{C}^h_{\mathbf{u}^{(f)}\mathbf{u}^{(f)}}(\mathbf{k},s)-\mathbf{C}^h_{\mathbf{u}^{(f)}\mathbf{v}}(\mathbf{k})\left(\mathbf{C}^h_{\mathbf{v}\mathbf{v}}(\mathbf{k},s)\right)^{-1}\mathbf{C}^h_{\mathbf{v}\mathbf{u}^{(f)}}(\mathbf{k},s)\right]\mathring{\mathbf{u}}^{(f)R}(\mathbf{k},s)+$$
$$-\left[\mathbf{C}^h_{\mathbf{u}^{(f)}\mathbf{v}}(\mathbf{k})\left(\mathbf{C}^h_{\mathbf{v}\mathbf{v}}(\mathbf{k},s)\right)^{-1}\mathbf{C}^h_{\mathbf{v}\mathbf{u}^{(b)}}(\mathbf{k},s)\right]\mathring{\mathbf{u}}^{(b)R}(\mathbf{k},s)=\mathring{\mathbf{f}}^{(f)}(\mathbf{k},s),$$
$$\left[\mathbf{C}^h_{\mathbf{u}^{(b)}\mathbf{u}^{(b)}}(\mathbf{k},s)-\mathbf{C}^h_{\mathbf{u}^{(b)}\mathbf{v}}(\mathbf{k})\left(\mathbf{C}^h_{\mathbf{v}\mathbf{v}}(\mathbf{k},s)\right)^{-1}\mathbf{C}^h_{\mathbf{v}\mathbf{u}^{(b)}}(\mathbf{k},s)\right]\mathring{\mathbf{u}}^{(b)R}(\mathbf{k},s)+$$
$$-\left[\mathbf{C}^h_{\mathbf{u}^{(b)}\mathbf{v}}(\mathbf{k})\left(\mathbf{C}^h_{\mathbf{v}\mathbf{v}}(\mathbf{k},s)\right)^{-1}\mathbf{C}^h_{\mathbf{v}\mathbf{u}^{(f)}}(\mathbf{k},s)\right]\mathring{\mathbf{u}}^{(f)R}(\mathbf{k},s)=\mathring{\mathbf{f}}^{(b)}(\mathbf{k},s). \tag{36}$$

The nonnull components of $\left(\mathbf{C}^h_{\mathbf{v}\mathbf{v}}(\mathbf{k},s)\right)^{-1}=\mathrm{adj}\left(\mathbf{C}^h_{\mathbf{v}\mathbf{v}}(\mathbf{k},s)\right)/\det\left[\mathbf{C}^h_{\mathbf{v}\mathbf{v}}\right.$ $\left.(\mathbf{k},s)\right]$, show poles at infinity in terms of s in correspondence of the zeros of the denominator which are associated to the presence of the resonators. Such frequencies approximate the central one of certain band gaps in the material frequency spectrum. As shown in Section 4, the continuum model can accurately capture the amplitude of all the band gaps of the metamaterial accurately, and the accuracy increases as the order of continualization increases. In the case of non homogeneous waves, since $s=\imath\omega$, with $\omega\in\mathbb{R}$, the frequency spectrum can be obtained from the intersection of two hypersurfaces immersed in $\mathbb{R}^5$, these lasts derived by imposing the vanishing of the real and imaginary components of the characteristic polynomial $\mathcal{P}^h(\mathbf{k},\omega)=\det[\mathbf{C}^h(\mathbf{k},\omega)]=\mathcal{P}^h_R(\mathbf{k},\omega)+\imath\,\mathcal{P}^h_I(\mathbf{k},\omega)$. Therefore

$$\begin{cases}\mathcal{P}^h_R(k_R,k_I,\theta_R,\theta_I,\omega)=0\\ \mathcal{P}^h_I(k_R,k_I,\theta_R,\theta_I,\omega)=0\end{cases} \tag{37}$$

If the Bloch wave is homogeneous ($\mathbf{n}_R=\mathbf{n}_I=\mathbf{n}$, or $\theta_R=\theta_I=\theta$), the dispersion spectrum of the continuum model results from the intersection of two hypersurfaces immersed in $\mathbb{R}^4$. Furthermore, by fixing the propagation direction $\mathbf{n}$ (or, equivalently, θ), these two hypersurfaces result to be immersed in $\mathbb{R}^3$, namely

$$\begin{cases}\mathcal{P}^h_R(k_R,k_I,\omega)=0\\ \mathcal{P}^h_I(k_R,k_I,\omega)=0\end{cases} \tag{38}$$

Alternatively, in all these cases the dispersion properties of the continuum model can be directly obtained from the resolution of the polynomial eigenproblem in $\mathbf{k}$ parameterized in ω expressed as $\mathbf{C}^h(\mathbf{k},\omega)\mathring{\mathbf{q}}^R(\mathbf{k},\omega) = \mathbf{0}$, since now $\mathbf{C}^h(\mathbf{k},\omega)$ is a polynomial in $\mathbf{k}$ of order $2N$. Finally, when the spatial attenuation of the wave is not taken into account, the wave vector $\mathbf{k}$ is such that $\mathbf{k} \in \mathbb{R}^2$ and dispersion spectra can be derived from the resolution of the quadratic eigenproblem parameterized in $\mathbf{k}$ in the form $\mathbf{C}^h(\mathbf{k},\omega)\mathring{\mathbf{q}}^R(\mathbf{k},\omega) = \mathbf{0}$, where ω is the eigenvalue and $\mathring{\mathbf{q}}^R(\mathbf{k},\omega)$ the eigenvector. Once again, if the Lagrangian system is constituted by a single layer without resonators, the field equations of the gradient-type continuum model in the $(\mathbf{k},s)$-space (31) simplify to

$$\sum_{r=0}^{2N}\sum_{p_1+p_2=r}\frac{1}{p_1!p_2!}k_1^{p_1}k_2^{p_2}\left\{\left.\frac{\partial^r\mathbf{D}\,F}{\partial k_1^{p_1}\partial k_2^{p_2}}\right|_{\mathbf{k}=\mathbf{0}}\mathring{\mathbf{u}}^R(\mathbf{k},s) + \mathbf{M}_s\left.\frac{\partial^r F}{\partial k_1^{p_1}\partial k_2^{p_2}}\right|_{\mathbf{k}=\mathbf{0}}s^2\mathring{\mathbf{u}}^R(\mathbf{k},s)\right\} = \mathring{\mathbf{f}}_s(\mathbf{k},s), \tag{39}$$

and the propagation and spatial attenuation of Bloch waves inside the discrete lattice for the non homogeneous and homogeneous waves cases can be investigated from the resolution of the eigenproblem

$$\sum_{r=0}^{2N}\sum_{p_1+p_2=r}\frac{1}{p_1!p_2!}k_1^{p_1}k_2^{p_2}\left\{\left.\frac{\partial^r F}{\partial k_1^{p_1}\partial k_2^{p_2}}\right|_{\mathbf{k}=\mathbf{0}}s^2\mathbf{M}_s + \left.\frac{\partial^r\mathbf{D}\,F}{\partial k_1^{p_1}\partial k_2^{p_2}}\right|_{\mathbf{k}=\mathbf{0}}\right\}\mathring{\mathbf{u}}^R(\mathbf{k},s) = \mathbf{0}. \tag{40}$$

3.2. Low frequency continualization

The procedure described in the following to obtain a low frequency continualization scheme departs from an asymptotic approximation of the frequency spectrum of the Lagrangian system. If the wave vector is expressed in polar coordinates as $\mathbf{k} = k_i\mathbf{e}_i = r\mathbf{n}$, with $r = \|\mathbf{k}\|_2$ the radial coordinate, and $\mathbf{n} = n_i\mathbf{e}_i = \cos\phi\,\mathbf{e}_1 + \sin\phi\,\mathbf{e}_2$ the unit vector written in terms of the angular coordinate $\phi = \arg\left(\mathbf{k}\cdot\mathbf{e}_1 + \imath\mathbf{k}\cdot\mathbf{e}_2\right)$, for a fixed value of ϕ, namely for a fixed wave propagation direction, the characteristic equation of the system (5) can be written as $F(\omega(r),r) = 0$, since $s = \imath\omega$. Furthermore, if only the propagation of the wave is taken into account, since the considered material is elastic, the wave vector is such that $\mathbf{k} \in \mathbb{R}^2$. To find an explicit solution for the characteristic equation, an asymptotic expansion of $\omega(r)$ in powers of r is employed around $r = 0$, namely

$$\omega(r) = \sum_{n\in\mathbb{N}}\omega^{[n]}r^n = \omega^{[0]} + \omega^{[1]}r + \omega^{[2]}r^2 + \cdots + \omega^{[n]}r^n + \cdots \tag{41}$$

The expansion (41) locally approximates the solution ω of the characteristic equation in the vicinity of $r = 0$, assuming that $\omega(r)$ has sufficient regularity. The implicit characteristic function $F(\omega(r),r)$ can then be regarded as a composite function $G(r)$ of a single variable, whose Taylor series expansion in powers of r reads

$$G(r) = \sum_{n\in\mathbb{N}}\frac{G^{[n]}}{n!}r^n = G^{[0]} + G^{[1]}r + \frac{G^{[2]}}{2}r^2 + \cdots + \frac{G^{[n]}}{n!}r^n + \cdots, \tag{42}$$

with $G^{[n]}$ the nth order derivative of G with respect to r evaluated at $r = 0$. The chain rule's recursive implementation is mandatory to differentiate the composite function $G(r)$. For example, evaluating the partial derivatives of F at $\omega = \omega^{[0]}$ and $r = 0$, coefficients $G^{[1]}$ and $G^{[2]}$ read

$$\begin{aligned} r^1 &: \; G^{[1]} = \omega^{[1]}\frac{\partial F(\omega,r)}{\partial\omega} + \frac{\partial F(\omega,r)}{\partial r},\\ r^2 &: \; G^{[2]} = 2\omega^{[2]}\frac{\partial F(\omega,r)}{\partial\omega} + \omega^{[1]^2}\frac{\partial^2 F(\omega,r)}{\partial\omega^2} + 2\omega^{[1]}\frac{\partial^2 F(\omega,r)}{\partial\omega\partial r} + \frac{\partial^2 F(\omega,r)}{\partial r^2}. \end{aligned} \tag{43}$$

The approximate characteristic equation $G(r) = 0$ is asymptotically satisfied equating to zero each coefficient $G^{[n]}$ at the order r^n in sequence, starting from the generating solution at the zeroth-order of $G^{[0]}(0) = 0$. The procedure leads to a sequence of perturbation equations, namely nth order equations, each in a single unknown, which is one of the sensitivities $\omega^{[n]}$. Details about the evaluation of coefficients $G^{[n]}$ can be found in Bacigalupo and Lepidi (2016), Fantoni and Bacigalupo (2020), where a recursive form for the nth sensitivity is provided. It is worth mentioning that, when a sensitivity $\omega_i^{[n]}$ has a multiplicity $m > 1$, the successive $m-1$ perturbation equations result undetermined and one must resort to the next mth perturbation problem to find $\omega_i^{[n+1]}$. Focusing the attention on the root $\omega = 0$, which is always, by definition, a solution for the generating problem and is such that $G^{[1]}$ results identically zero, the solution obtained for the characteristic equation $G(r) = 0$ accomplishing a second-order approximation has been identified with the characteristic equation of a first-order (Cauchy) equivalent continuum, reading

$$\det\left[\tilde{\boldsymbol{C}}(\mathbf{k}\otimes\mathbf{k}) - \vartheta\omega^2\mathbf{I}\right] = \det\left[r^2\tilde{\boldsymbol{C}}(\mathbf{n}\otimes\mathbf{n}) - \vartheta\omega^2\mathbf{I}\right] = 0. \tag{44}$$

In Eq. (44), $\tilde{\boldsymbol{C}} = \tilde{C}_{ipq_1q_2}\mathbf{e}_i\otimes\mathbf{e}_p\otimes\mathbf{e}_{q_1}\otimes\mathbf{e}_{q_2}$ and $\tilde{C}_{ipq_1q_2} = C_{iq_1pq_2}$ with $C_{iq_1pq_2}$ the components of the unknown fourth-order elastic tensor $\boldsymbol{C}$, ϑ is the overall mass density, which is simply the total mass of the system divided by the volume, and $\mathbf{I}$ is the second-order identity operator. Equating the quadratic Eq. (44) with the one obtained through the single-parameter perturbative technique just described for the discrete lattice, a nonlinear system of algebraic equations is obtained for each wave propagation direction considered. Taking care to select those solutions leading to a positive defined tensor $\boldsymbol{C}$, the quadratic eigenproblem (44), where the frequency ω is the eigenvalue, gives the low frequency approximation of the Lagrangian system spectrum. As shown in the following, the slope of the acoustic branches is accurately captured by the identification here described for all the considered systems. It is worth observing that the low frequency continualization can be performed by identifying the spectrum of the first-order equivalent medium with the one deriving from the gradient-type continuum model (32) truncated at the second-order.

4. Illustrative example: the case of a multilayered antitetrachiral metamaterial

The continualization technique described above is here particularized to multilayered metamaterials having an antitetrachiral topology. As known, antitetrachiral materials are phenomenologically characterized by a marked auxetic macroscopic elastic response (Bacigalupo and Lepidi, 2016). The auxeticity, mechanically described by negative values of the Poisson's ratio, manifests with the fascinating and counterintuitive behavior of expanding laterally when a longitudinal stretch is applied and, conversely, contracting laterally when these materials are compressed (Dirrenberger et al., 2013; Prawoto, 2012; Greaves et al., 2011; Alderson and Alderson, 2007; Evans and Alderson, 2000; Lakes, 1991). One considers the bi-layered lattice material depicted in Fig. 3: each layer is characterized by an antitetrachiral topology in which four equi-spaced rings of radius R are connected by four ligaments of length L, cross sectional area A and moment of inertia J. One layer is rotated with respect to the other one by an angle equal to $\pi/2$ and the lattice coordination number is equal to $n = 4$ for each stratum. In antitetrachiral systems, the same side of the ligaments is connected to adjacent rings, so opposite chiralities characterize the nearest neighboring rings.

Adopting the following dimensionless parameters describing the geometry of each antitetrachiral layer

$$\chi_s = \sqrt{\frac{J_s}{M_s L^2}} = \frac{1}{9}, \qquad \rho = \sqrt{\frac{J}{A L^2}} = \frac{1}{10}, \qquad \delta = \frac{2R}{L} = \frac{1}{10}, \tag{45}$$

and the following dimensionless quantities characterizing the resonators

$$\varsigma_d = \frac{\kappa_d}{E L} = \frac{2}{100}, \qquad \varsigma_\theta = \frac{\kappa_\theta}{E L^2} = \frac{2}{100}, \qquad \chi_r = \sqrt{\frac{J_r}{M_r L^2}} = \frac{1}{10}, \tag{46}$$

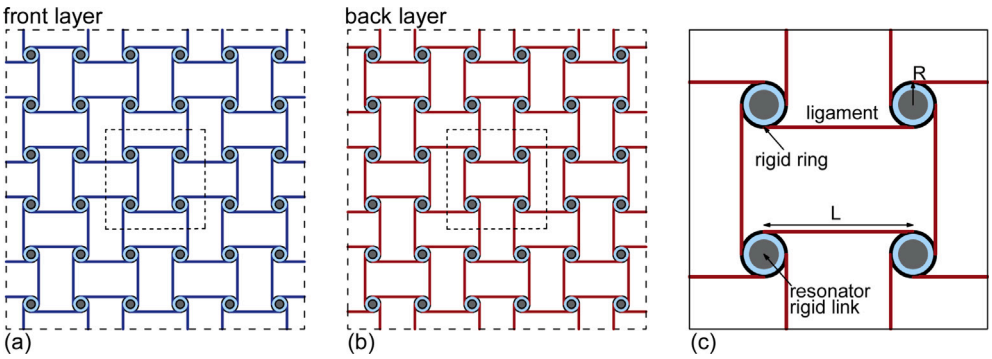

Fig. 3. Multilayered lattice material with antitetrachiral topology: front layer (a), back layer (b), and periodic cell of the back layer (c).

since $s = \imath\omega$, with $\omega \in \mathbb{R}$, and $\mathbf{K}_{sr}^{(f)} = \mathbf{K}_{sr}^{(b)} = \mathbf{K}_{rs}^{(f)} = \mathbf{K}_{rs}^{(b)}$, the nonnull components of the matrix $\mathbf{A} = \mathbf{K}_{sr}\mathbf{B}^{-1}(s)\mathbf{K}_{rs}$ (see Eq. (7)), are plotted in Fig. 4 in terms of nondimensional frequency ω/ω_c, with $\omega_c = \sqrt{EA/(M_s L)}$, and of the ratio $\eta = M_r/Ms$ between the mass of each resonator and the mass of each stiff ring. If the surfaces of Figs. 4-(a) and 4-(c) are sectioned in correspondence of $\eta = 1/10$, $\eta = 1$, and $\eta = 10$ one obtains the curves of Figs. 4-(b) and 4-(d). In the following, the parameter η is set equal to 1, value in correspondence of which both the components A_{11} and A_{33} show vertical asymptotes for a ratio $\omega/\omega_c = 141/100$, which is one of the resonator's nondimensional natural frequency $\sqrt{k_d/M_r}/\omega_c$. Relative ring-resonator translational and rotational stiffness κ_d and κ_θ could be calibrated using simple procedures as the one described in Appendix A of Bacigalupo and Gambarotta (2016). The explicit expression of the components of the mass matrices $\mathbf{M}_s^{(\ell)}$, $\mathbf{M}_r^{(\ell)}$ and of the stiffness-like matrices $\mathbf{K}_{ss}^{(\ell)}$, $\mathbf{K}_{sr}^{(\ell)} = \mathbf{K}_{rs}^{(\ell)}$, $\mathbf{K}_{rr}$, $\mathbf{K}_{ss_j}^{+(\ell)}$, and $\mathbf{K}_{ss_j}^{-(\ell)}$ are detailed in Appendix A for the antitetrachiral topology at hand. The free wave propagation of Bloch waves inside the metamaterial is investigated employing Eq. (5) with null source terms ($\mathring{\mathbf{f}} = \mathbf{0}$) or, alternatively, using system (10), since $s = \imath\omega$. As an illustrative example, Fig. 5 plots the frequency spectrum obtained in the case of a homogeneous wave propagating along directions $\mathbf{n} = \mathbf{e}_1$ and $\mathbf{n} = -\mathbf{e}_1/\sqrt{2} - \mathbf{e}_2/\sqrt{2}$ where the spatial damping of the wave is not taken into account ($\mathbf{k} \in \mathbb{R}^2$). In particular, the nondimensional frequency ω/ω_c is depicted in terms of the nondimensional curvilinear abscissa ξ. As represented in Fig. 5-(b), this last runs from vertex A=$(-\pi, -\pi)$ of the first dimensionless Brillouin zone, to point B = $(0, 0)$ till reaching the point C = $(\pi, 0)$. Black curves refer to the discrete frequency spectrum obtained by solving the quadratic eigenproblem (11) in $\mathbf{k}$. The blue curves refer to the fourth-order ($2N = 4$) standard-like continualization case and plot the solution of the eigenproblem (32) with $\mathring{\mathbf{f}} = \mathbf{0}$ and unitary regularization kernel. Finally, red curves plot the frequency spectrum of a second-order homogenized continuum obtained through the enhanced technique and determined again by means of the eigenproblem (32) with null source terms. The Figs. 5-(a),(c), and (d) refer to the case of a single antitetrachiral layer without resonators, while Figs. 5-(e), (g), and (h) refer to the case of a bi-layered antitetrachiral lattice with resonators, as depicted in Fig. 3. As one can notice, both the standard-like and the enhanced continualization techniques give a perfect correspondence of spectrum with respect to the Lagrangian case around $\xi = 0$ and, as expected, they tend to move apart from the discrete case as the curvilinear abscissa moves away from the origin. Furthermore, it is evident that the standard-like continualization brings to frequency spectra in which the curves are characterized by a vertical tangent for $\xi = -\sqrt{2}\pi$ and $\xi = \pi$, therefore infinite group velocity. The enhanced continualization is not characterized by this pathology, as stressed in the zooms of Figs. 5-(c),(d),(g), and (h). In the case of a bi-layered antitetrachiral topology it is also possible to note the opening of two low-frequency further band gaps with respect to the single-layer case. Such band gaps have nondimensional central frequencies equal to $\omega/\omega_c \approx 118/100$ and $\omega/\omega_c \approx 138/100$, this last approximately corresponding to one of the resonator's nondimensional natural frequency that, as already mentioned and showed in Fig. 4, is equal to $\sqrt{k_d/M_r}/\omega_c = 141/100$. The geometrical and material parameters of the bilayered case could be subjected to an optimization procedure to determine the parameters combination that maximizes, for example, the amplitude of low-frequency band gaps (Fantoni et al., 2023). This is, of course, out of the scope of the present work. Referring to the enhanced continualization only, in Fig. 6 it is shown how, increasing the continualization order, the frequency spectrum of the continuum model converges more and more to the one of the discrete model, this last represented by black curves. In particular, red curves refer to a fourth-order continualization ($2N = 4$), green ones to an eighth-order continualization ($2N = 8$), and magenta curves refer to a sixteenth-order continualization ($2N = 16$). As is even more evident from the zooms that have been made in the Figs. 6-(c),(d),(g), and (h), the frequency spectrum of an eighth-order continuum model (magenta curves) traces the discrete one almost throughout the entire range of ξ. Figs. 6-(a),(c), and (d) correspond to the single-layer case with antitetrachiral topology and no resonators, while Figs. 6-(e),(g), and (h) plot the frequency spectrum for the bi-layered case with resonators. Always referring to the homogeneous wave case, Fig. 7 plots the absolute value of the phase velocity $v_p^{\mathbf{n}}$ with respect the nondimensional frequency ω/ω_c for the discrete medium (black curves), and the enhanced continuum model with continualization order $2N = 4$ (red curves), $2N = 8$ (green curves), and $2N = 16$ (magenta curves). Figs. 7-(a) and 7-(b) refer to the single-layer case, while Figs. 7-(c) and 7-(d) to the bi-layered metamaterial. Figs. 7-(a) and 7-(c) plot the phase velocity for $\xi \in [-\sqrt{2}\pi, 0]$, while Figs. 7-(b) and 7-(d) plot the phase velocity for $\xi \in [0, \pi]$. It is confirmed, once again, the accuracy reached by the continuum model in capturing the dynamic behavior of the corresponding discrete medium. Furthermore, it is evident how the amplitude of all the band gaps, here represented by gray rectangles, is truthfully caught by the continuum models.

When spatial damping is taken into account, the wave vector has complex components. Fig. 8 plots the frequency spectrum obtained considering a wave propagation direction $\mathbf{n} = \mathbf{e}_1$. In particular, black curves refer to the spectrum of the Lagrangian system, obtained by solving a quadratic eigenproblem in the Floquet multiplier $\lambda_{\mathbf{n}}$ (see Appendix A Eq. (57)), and then recalling that the complex dimensionless wave number is equal to $l_r\kappa = l_r(\kappa_R + \imath\,\kappa_I) = \ln(\lambda_{\mathbf{n}})/\imath$, where, from now on, the reference length is defined as $l_r = 2L$. Red curves, instead, refer to the fourth-order enhanced continualization scheme, for which the frequency spectrum is obtained by solving the polynomial eigenproblem (32) with null source terms. The Fig. 8 stresses again the very good agreement obtained between the discrete and the homogenized model, which can be further improved by increasing the continualization order. Figs. 8-(a) and (b) refer to the single antitetrachiral layer, while Figs. 8-(c) and (d) to the bi-layered case. Furthermore, Figs. 8-(b) and (d) are planar representations in the plane (κ_I, ω) of the corresponding three-dimensional spectra, inserted to make clear the frequency ranges

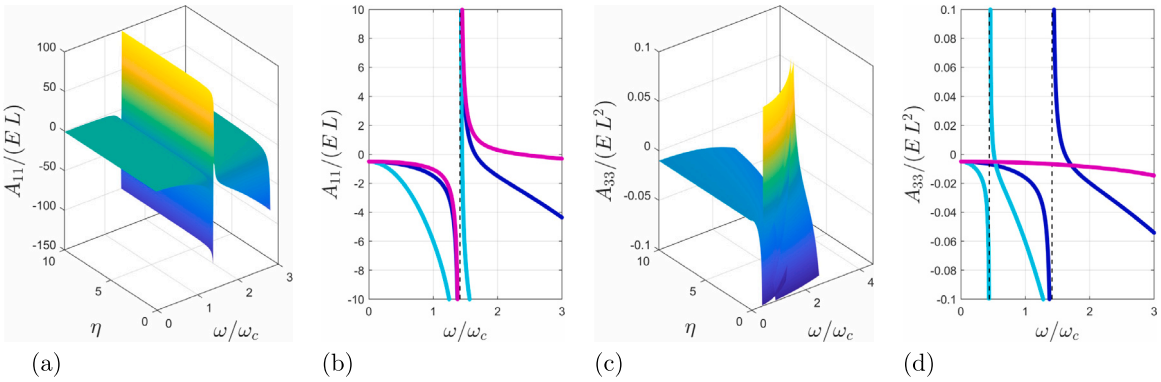

Fig. 4. (a)–(c): nondimensional nonnull components of the matrix $\mathbf{A}$ in terms of ω/ω_c and the ratio $\eta = M_r/M_s$. (b)–(d): sections of the corresponding 3D plots for $\eta = 1/10$ (cyan curves), $\eta = 1$ (blue curves), and $\eta = 10$ (magenta curves).

in which there are band gaps, these lasts characterized by $\kappa_I \neq 0$. Finally, for the same wave propagation direction $\mathbf{n} = \mathbf{e}_1$, Fig. 9 represents the real and imaginary components of the Floquet multiplier $\lambda_{\mathbf{n}} = \lambda_{\mathbf{n}_R} + \imath\,\lambda_{\mathbf{n}_I}$, obtained for the discrete model (black dots) by the resolution of the quadratic eigenvalue problem $\mathbf{C}(\lambda_{\mathbf{n}}, \omega)\mathring{\mathbf{q}}(\lambda_n, \omega) = \mathbf{0}$ and for the fourth-order enhanced continualization (red dots) by means of the relation $\lambda_{\mathbf{n}} = \exp(\imath\,\kappa\, l_r)$. Fig. 9-(a) refers to the single-layer case, while Fig. 9-(b) to the bi-layered one. Both of them refer to a dimensionless frequency $\omega/\omega_c \in [0, 1]$ and show that, when a curve in the frequency spectrum belongs to the propagation plane ($k_I = 0$), the components of the Floquet multiplier $\lambda_{\mathbf{n}}$ wrap around the unitary cylinder, depicted in gray, while when $k_I \neq 0$ the components of $\lambda_{\mathbf{n}}$ do not belong to the lateral surface of such cylinder.

The low frequency continualization described in Section 3.2 is here employed to identify the equivalent first-order medium for the single-layer case. Starting from the single-parameter perturbative technique applied for the spectrum of the discrete system, the following asymptotic expansions for $\omega_i^{\pm}(r)$, with $i = 1, 2$, have been obtained in terms of the parameters (45). They read

$$\omega_i^{\pm} = (-1)^{i+1}\, l_r\, r \left(\alpha^{(2,0)} n_1^2 + \alpha^{(0,2)} n_2^2 \pm \left(\alpha^{(4,0)} n_1^4 + \alpha^{(2,2)} n_1^2 n_2^2 + \alpha^{(0,4)} n_2^4\right)^{1/2}\right)^{1/2}, \tag{47}$$

with

$$\begin{aligned}
\alpha^{(2,0)} &= \alpha^{(0,2)} = \frac{\omega_c^2}{16(\delta^2 + 4\rho^2)} \left(\left(12\rho^2 + 1\right)\delta^2 + 48\rho^4 + 8\rho^2\right), \\
\alpha^{(2,2)} &= \frac{18\omega_c^4}{(\delta^2 + 4\rho^2)^2} \left(\frac{1}{16}\left(\rho^2 - \frac{1}{12}\right)^2 \delta^4 + \left(\frac{1}{2}\rho^6 + \frac{1}{24}\rho^4 - \frac{1}{144}\rho^2\right)\delta^2 \right. \\
&\quad \left. + \rho^8 + \frac{1}{3}\rho^6 - \frac{1}{36}\rho^4\right), \\
\alpha^{(4,0)} &= \alpha^{(0,4)} = \frac{9\omega_c^4}{(\delta^2 + 4\rho^2)^2} \left(\left(\frac{1}{4}\rho^2 - \frac{1}{48}\right)\delta^2 + \rho^4 - \frac{1}{6}\rho^2\right)^2.
\end{aligned} \tag{48}$$

For the first-order medium, the solution of the characteristic Eq. (44) leads to the frequencies $\omega_i^{\pm}$, with $i = 1, 2$, in terms of the components of the overall elasticity tensor $\boldsymbol{C}$ and of the overall mass density ϑ. They have the following expression

$$\omega_i^{\pm} = (-1)^{i+1}\, r \left(A^{(2,0)} n_1^2 + A^{(0,2)} n_2^2 \pm \left(A^{(4,0)} n_1^4 + A^{(2,2)} n_1^2 n_2^2 + A^{(0,4)} n_2^4\right)^{1/2}\right)^{1/2}, \tag{49}$$

with

$$\begin{aligned}
A^{(2,0)} &= A^{(0,2)} = \frac{\omega_c^2}{2\vartheta^2}\left(C_{1111} + C_{1212}\right), \\
A^{(2,2)} &= -\frac{\omega_c^4}{2\vartheta^4}\left(C_{1111}^2 - 2C_{1122}^2 - C_{1212}^2 + \left(-2C_{1111} - 4C_{1122}\right)C_{1212}\right), \\
A^{(4,0)} &= \frac{\omega_c^4}{4\vartheta^4}\left(C_{1111} - C_{1212}\right)^2.
\end{aligned} \tag{50}$$

The identification of Eqs. (47) and (49) allows attaining a nonlinear system of three algebraic equations whose unknowns are, because of the material constitutive cubic symmetry properties, the three independent components of the overall elastic tensor $\boldsymbol{C}$. Four different sets of solutions have been obtained and selecting the one that leads to the unique positive defined overall elastic tensor, the obtained $\boldsymbol{C}$ in an equivalent matrix form reads

$$\begin{aligned}
\boldsymbol{C} &= \begin{bmatrix} C_{1111} & C_{1122} & \sqrt{2}C_{1112} \\ C_{2211} & C_{2222} & \sqrt{2}C_{2212} \\ \sqrt{2}C_{1211} & \sqrt{2}C_{1222} & 2C_{1212} \end{bmatrix} \\
&= l_r^2 \vartheta \omega_c^2 \begin{bmatrix} \frac{1}{8}\frac{\delta^2+8\rho^2}{\delta^2+4\rho^2} & -\frac{1}{8}\frac{\delta^2}{\delta^2+4\rho^2} & 0 \\ -\frac{1}{8}\frac{\delta^2}{\delta^2+4\rho^2} & \frac{1}{8}\frac{\delta^2+8\rho^2}{\delta^2+4\rho^2} & 0 \\ 0 & 0 & 2\frac{3}{2}\rho^2 \end{bmatrix}.
\end{aligned} \tag{51}$$

Since the overall density ϑ is known and defined as the total mass of the system divided by its total volume, once the components of $\boldsymbol{C}$ are known, the frequency spectrum of the Cauchy equivalent medium can be obtained for all the wave propagation directions considered. Fig. 10-(a) compares the spectrum previously obtained for the Lagrangian system (black curves) and for the second-order enhanced continuum model (red curves) with the one of the first-order medium. Magenta curves are related to longitudinal waves, whereas blue ones are related to shear waves. Both of them accurately capture the slope of the acoustic branches of the spectrum for the two wave propagation directions considered, namely $\mathbf{n} = -\mathbf{e}_1/\sqrt{2} - \mathbf{e}_2/\sqrt{2}$ and $\mathbf{n} = \mathbf{e}_1$. The equivalent first-order medium can thus accurately describe the low frequency propagation of waves in the long wavelength regime. The Fig. 10-(b) is a three-dimensional representation of the spectrum of the Cauchy medium in the entire first Brillouin zone, with the indication of the curves represented in the Fig. 10-(a) along the selected propagation directions.

4.1. Forced wave propagation

The ability of the continualization scheme to capture the forced response of the system is here investigated, without losing generality, by applying a single punctual excitation to the first node of the $\mathcal{J}$-th periodic cell of the single antitetrachiral layer. Specifically, the mono-harmonic component $\mathbf{f}_{s_{\mathcal{J}}}(t) = \mathbf{F}H(t)\exp(St)$ is considered, having constant amplitude $\mathbf{F}$, purely imaginary excitation frequency $S = \imath\Omega$, and $H(t)$ representing the Heaviside function. The vector $\mathbf{F}$ is assumed to have all the components with a null value except the first one, which is equal to F, with a value such that $F/(EA) = 4762$. Because of this choice, the application of a bilateral Laplace transform in time and a bilateral $\mathcal{Z}$-transform in space, the forcing term results to be independent upon $\mathbf{z}$ and reads $\mathring{\mathbf{f}}_s(s) = \mathbf{F}/(s - S)$. The forced response

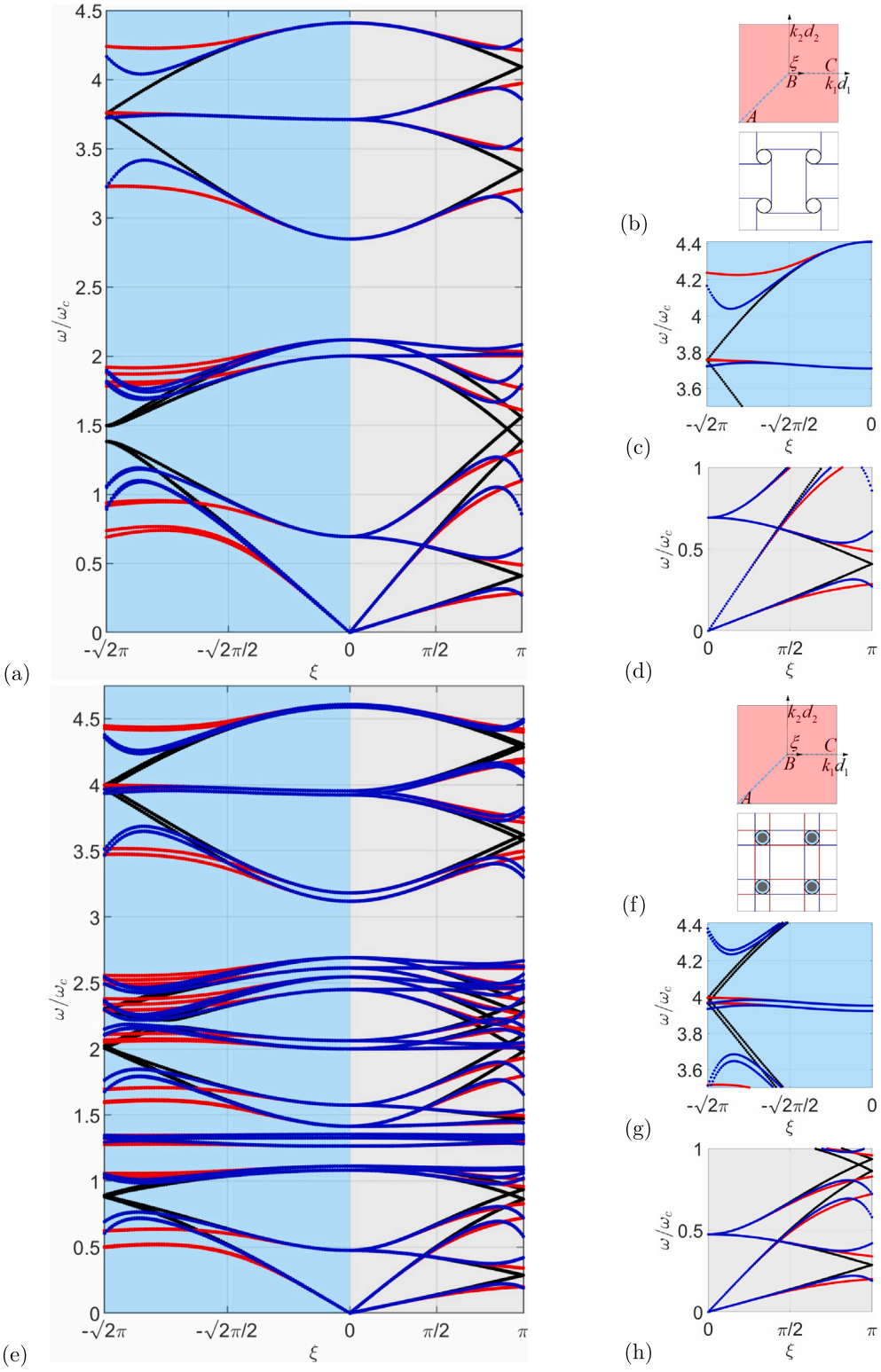

Fig. 5. ω/ω_c vs ξ for the discrete model (black), the fourth-order standard-like continualization (blue), and the fourth-order enhanced continualization (red). Single-layer case (a); first Brillouin zone and periodic cell (b); zoom for $\xi \in [-\sqrt{2}\pi, 0]$ and $\omega/\omega_c \in [3.5, 4.4]$ (c); zoom for $\xi \in [0, \pi]$ and $\omega/\omega_c \in [0, 1]$ (d). Bi-layered case (e); first Brillouin zone and periodic cell (f); zoom for $\xi \in [-\sqrt{2}\pi, 0]$ and $\omega/\omega_c \in [3.5, 4.4]$ (g); zoom for $\xi \in [0, \pi]$ and $\omega/\omega_c \in [0, 1]$ (h).

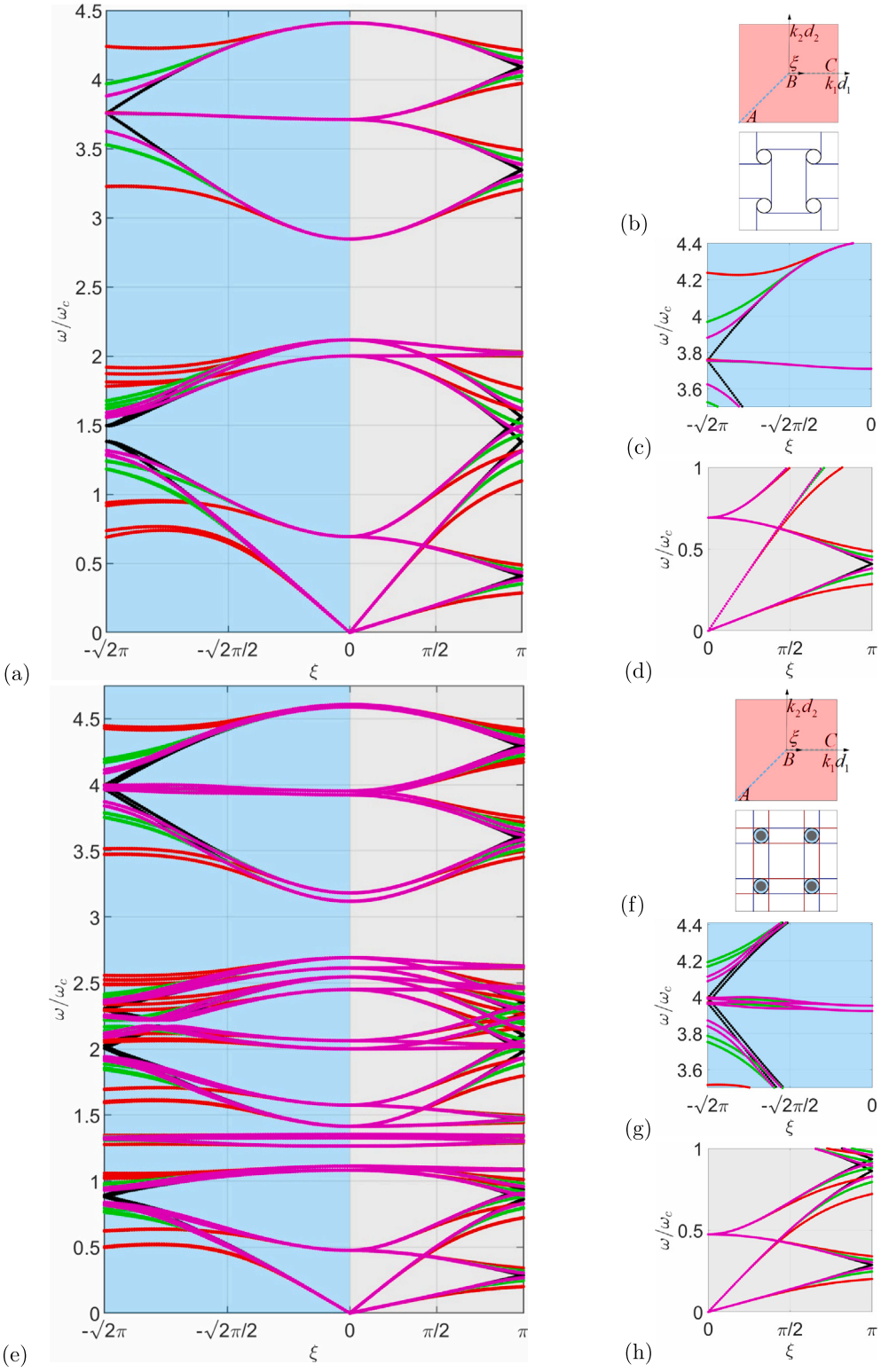

Fig. 6. ω/ω_c vs ξ for the discrete model (black), the enhanced continualization scheme with $2N = 4$ (red), $2N = 8$ (green), and $2N = 16$ (magenta). Single-layer case (a); first Brillouin zone and periodic cell (b); zoom for $\xi \in [-\sqrt{2}\pi, 0]$ and $\omega/\omega_c \in [3.5, 4.4]$(c); zoom for $\xi \in [0, \pi]$ and $\omega/\omega_c \in [0, 1]$ (d). Bi-layered case (e); first Brillouin zone and periodic cell (f); zoom for $\xi \in [-\sqrt{2}\pi, 0]$ and $\omega/\omega_c \in [3.5, 4.4]$(g); zoom for $\xi \in [0, \pi]$ and $\omega/\omega_c \in [0, 1]$ (h).

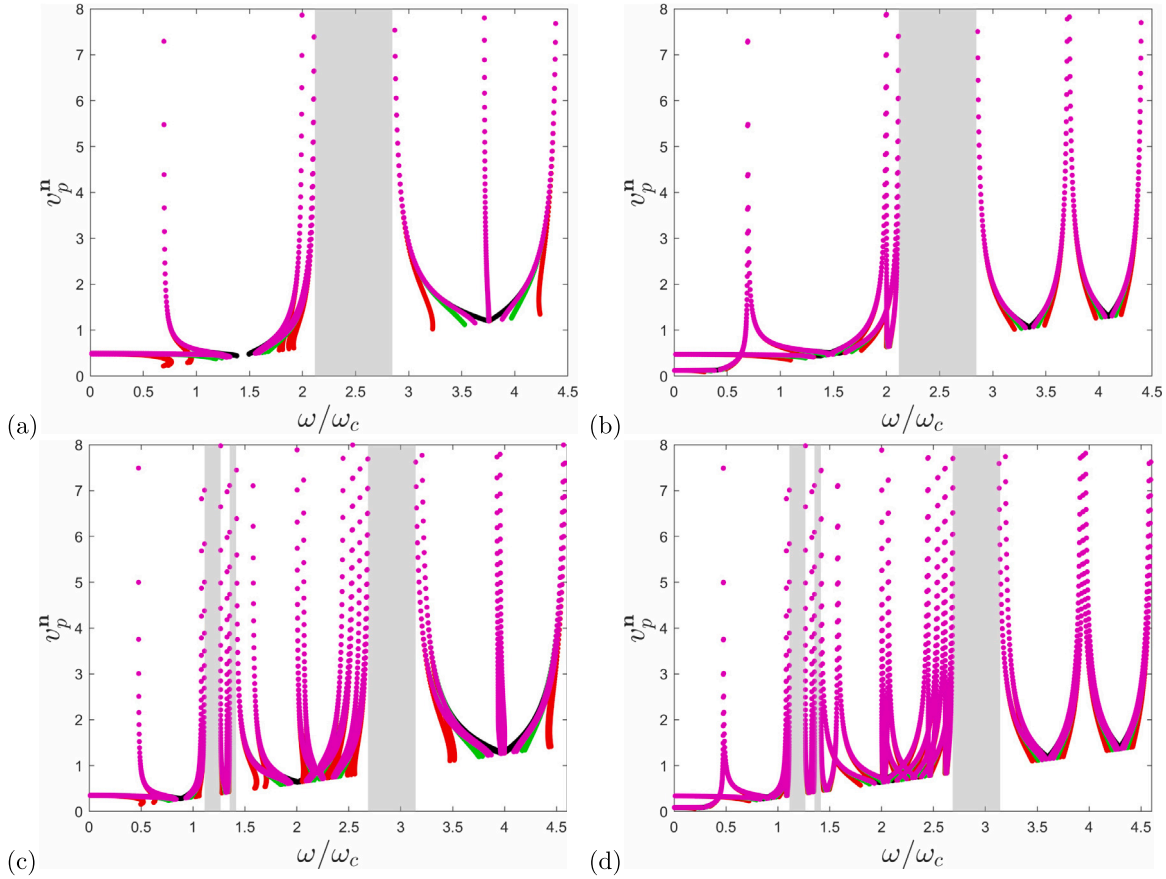

Fig. 7. Absolute value of the phase velocity $v_p^{\mathbf{n}}$ vs ω/ω_c for the discrete model (black), the enhanced continualization scheme of order $2N = 4$ (red), $2N = 8$ (green), and $2N = 16$ (magenta). Single-layer case (a)–(b), and bi-layered case (c)–(d). $\xi \in [-\sqrt{2}\pi, 0]$ (a)–(c), $\xi \in [0, \pi]$ (b)–(d). Gray rectangles represent the band gaps.

for the Lagrangian system is obtained by solving system (5) simplified for the single-layer case. Assuming that spatial damping is present, that $\mathbf{n} = \mathbf{e}_1$, and that both the excitation frequency and the fixed system frequency s fall within the first pass band of the material spectrum with $\Omega/\omega_c = 1.8$ and $\omega/\omega_c = 1$, Fig. 11-(b) plots the system response in terms of the nondimensional imaginary and real components of k_1. In particular, the dimensionless magnitude $|\mathring{q}_1|/L$ of the first component of vector $\mathring{\mathbf{q}}$ is plotted. All the singularity points associated with the poles at infinity are identified by black points in Fig. 11-(a), representing the zeros of the denominator of $|\mathring{q}_1|$, which are the intersections of the real (continuous blue curves) and imaginary (dashed blue curves) parts of the denominator itself. The intersections of the red curves in Fig. 11-(a), instead, correspond to the zeros of the real (continuous lines) and imaginary (dashed lines) components of the numerator of $|\mathring{q}_1|$. Such intersections do not overlap to the zeros of the denominator. It is evident how the forced response of the enhanced continuum model approximates the one of the Lagrangian system and how the accuracy of the approximation, as expected, increases as the order of continualization increases. Figs. 11-(c)–(d) correspond to the enhanced continualization model with $2N = 4$, while Fig. 11-(e)–(f) to the case $2N = 16$. Finally, Fig. 12 compares the responses of the Lagrangian system (black curves), and the ones of the enhanced continuum model with $2N = 4$ (red curves), and $2N = 16$ (magenta curves) for three different values of $k_{1_R} l_r$, namely $\pi/4$, $\pi/2$, and $7/10\pi$. While the second-order continuum model well captures the system's behavior far away from the poles at infinity, the eighth-order continuum model can very well approximate the forced response along all the range of k_{1R}. Finally, by means of an inverse bilateral Laplace transform, the time-dependent response $\tilde{q}_1(\mathbf{k}, t) = \mathcal{L}^{-1}\left[\mathring{q}_1(\mathbf{k}, s)\right]$ is determined for a fixed value of the wave vector. The Fig. 13 plots the response attained at $\mathbf{k} = \mathbf{0}$ for the discrete system and the two continuum models with $2N = 4$ and $2N = 16$. The curves perfectly overlap over the entire time range considered. It is worth observing that, for a fixed continualization order, the accuracy deteriorates as the components of $\mathbf{k}$ increase, but the response of the continuum model converges to the Lagrangian's one as $2N$ increases. The response of the integro-differential continuum model, instead, coincides with the one of the discrete system for each value of $\mathbf{k}$ by definition.

5. Conclusions

The present work focuses on the dynamic continualization of multifield multilayered discrete systems with lumped masses in order to provide continuum models able to achieve an accurate characterization of the frequency spectrum of the corresponding lattice material. The adopted continualization scheme is based on a general mathematical framework grounded on integral transforms or pseudo-differential operators which allow to capture the essential aspects of the physical problem under investigation. Obtained continuum models are described by both integral-type and higher-order gradient-type governing equations obtained through an enhanced continualization of the equations of motion of the Lagrangian model. The enhanced continualization procedure proves to be energetically consistent in the definition of the overall non-local constitutive and inertial terms and obtained Floquet–Bloch spectra are not affected by the pathologies characterizing the standard-like continualization. This last is defined using a unitary regularization kernel and provides the identification of gradient-type continuum models with local inertial terms which, in general, show dynamical instabilities in the short-wave limit, both for the acoustic and the optical branches of the spectrum. Dispersion curves determined

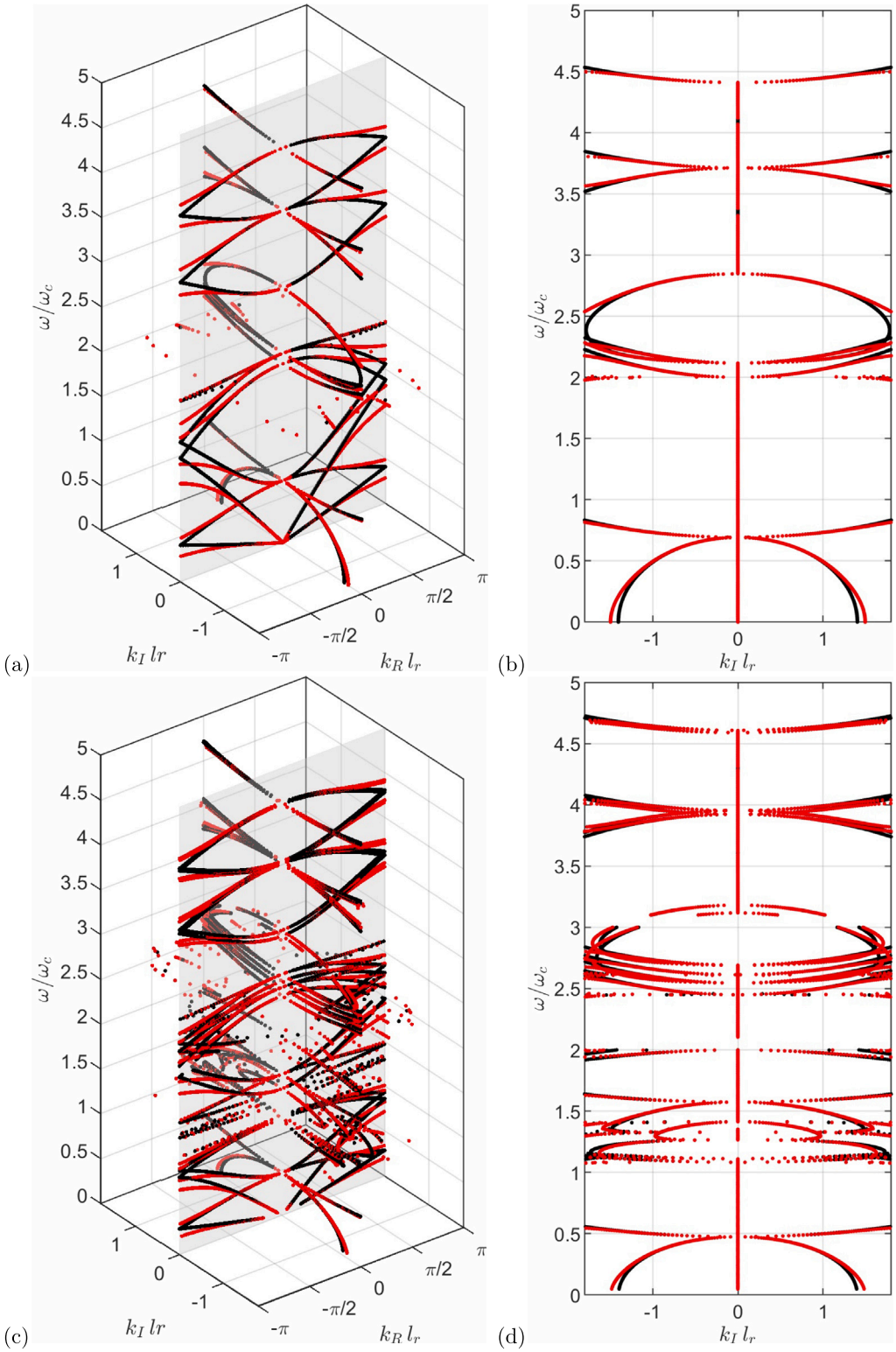

Fig. 8. Imaginary and real components of the dimensionless wave vector $\kappa_I l_r$ and $\kappa_R l_r$ vs ω/ω_c for the discrete model (black) and the fourth-order enhanced continualization (red). Three-dimensional representation for the single-layer case (a) and its planar projection onto the plane $(k_I\, l_r, \omega/\omega_c)$ (b). Three-dimensional representation for the bi-layered case (c) and its planar projection onto the plane $(k_I\, l_r, \omega/\omega_c)$ (d).

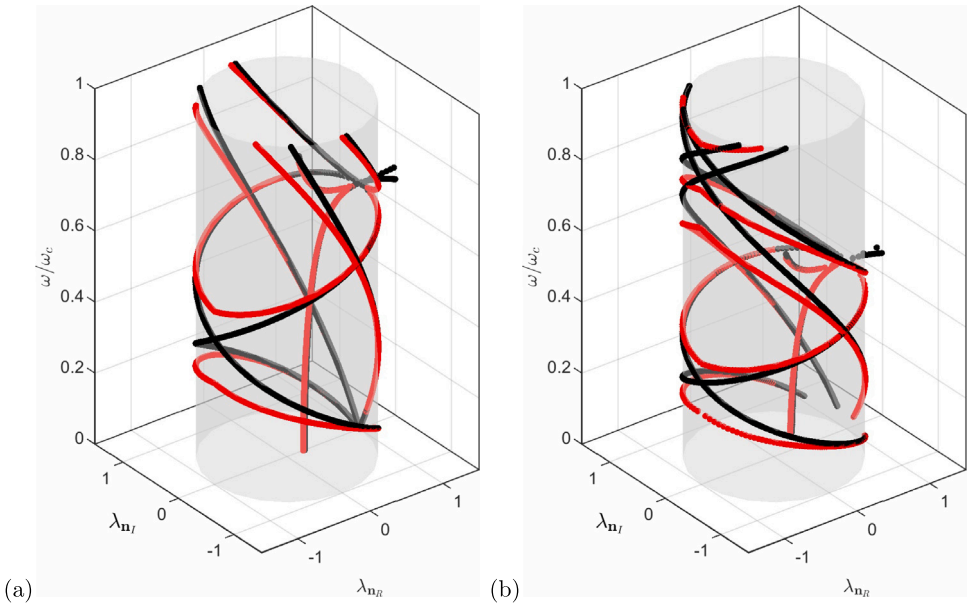

Fig. 9. Imaginary and real components $\lambda_{\mathbf{n}_I}$ and $\lambda_{\mathbf{n}_R}$ of the Floquet multiplier vs $\omega/\omega_c \in [0,1]$ for the discrete model (black) and the fourth-order enhanced continualization (red). Single-layer case (a), and bi-layered one (b).

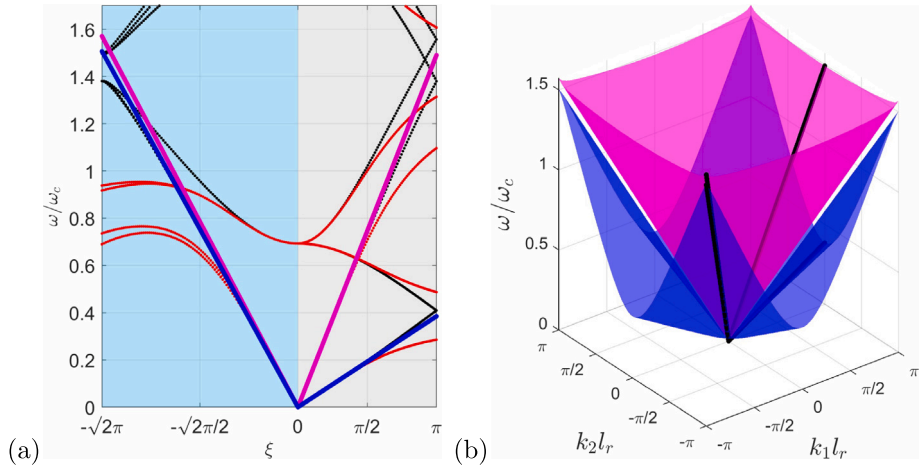

Fig. 10. (a) ω/ω_c vs curvilinear abscissa ξ for the discrete single-layer case (blue curves), the second order enhanced continuum model (red curves), and the first-order homogenized medium (magenta curves associated to longitudinal waves and blue curves to shear ones). (b) Three-dimensional frequency spectrum for the equivalent Cauchy medium.

by the enhanced continualization, instead, do not show infinite group velocities at the boundaries of the first Brillouin zone. A unitary regularization kernel is analytic everywhere in the complex space, while the regularization kernel adopted in the enhanced model has been conceived in order to show polar singularities at the boundary of the first Brillouin zone in correspondence of the lattice coordination directions. Consequently, the kernel results to be analytic only in a subdomain of the complex space, whose characteristic dimension is governed by the distance between the point around which its Taylor series approximation is centered and the polar singularities at the boundary of the Brillouin zone. Then, since the frequency spectrum is periodic along the real component of the wave vector, the spectrum obtained in the first Brillouin zone can be extended along the entire real domain of the wave numbers. Continuum models of increasing orders are formulated through a formal Taylor series expansion of the integral kernels or the corresponding pseudo-differential functions accounting for shift operators. The frequency spectrum converges to the one of the discrete system as the truncation order along the lattice coordination directions increases. An excellent quantitative agreement between the frequency spectrum of the continuum model and the one of the discrete lattice material has been shown by taking into account two different cases: an antitetrachiral lattice topology with four lumped masses at the nodes and two antitetrachiral layers placed one on top of the other connected by local resonators. Propagation and spatial attenuation of Bloch waves have been investigated by solving the corresponding eigenproblem either in terms of frequency, or in terms of wave vector, or, alternatively, in terms of the corresponding Floquet multiplier. A low frequency continualization is also presented. Starting from an asymptotic approximation of the frequency spectrum of the lattice material, the components of the elastic tensor of a first-order, energetically consistent, equivalent medium have been provided by means of the identification of the relative characteristic equations. As expected, the spectrum of the Cauchy equivalent medium accurately approximates the slope of the acoustic branches of the discrete system's frequency spectrum, Finally, the high-frequency continualization scheme has been employed in order to approximate the forced response of the materials, confirming the capabilities of the enhanced continualization to accurately represent the dynamic behavior of the lattice material.

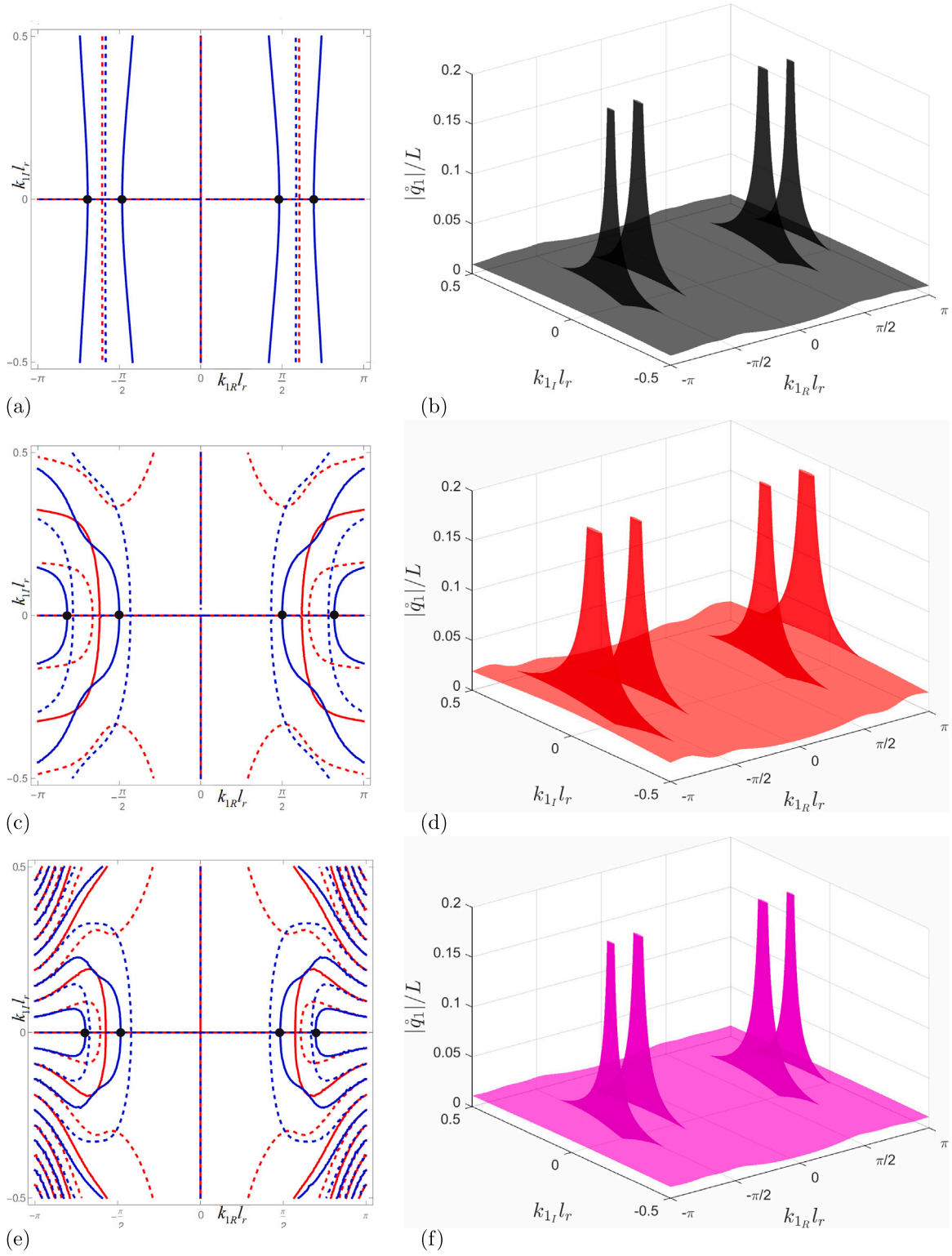

Fig. 11. Singularity points of the response $\mathring{q}_1$ and dimensionless magnitude of $\mathring{q}_1$ in terms of $k_{1_R} lr$ and $k_{1_I} l_r$ for the Lagrangian system (a)–(b), and the enhanced continuum models with $2N = 4$ (c)–(d), and $2N = 16$ (e)–(f).

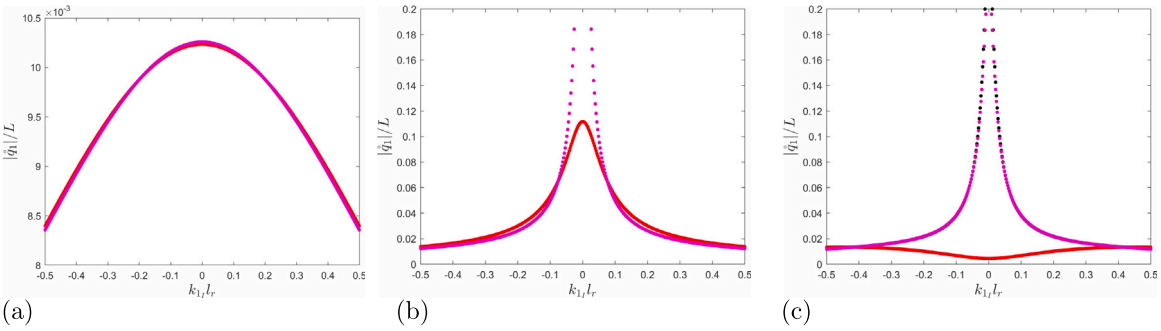

Fig. 12. Dimensionless magnitude of $\mathring{q}_1$ vs $k_{1_I} l_r$ at $k_{1_R} l_r = \pi/4$ (a), $k_{1_R} l_r = \pi/2$ (b), $k_{1_R} l_r = 7/10\pi$ (c) for the Lagrangian system (black curves), and the enhanced continuum models with $2N = 4$ (red curves), and $2N = 16$ (magenta curves).

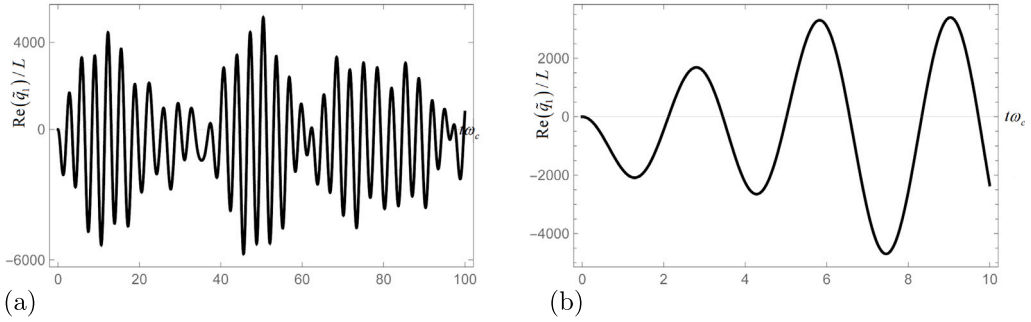

Fig. 13. (a) Dimensionless real part of the response $\tilde{q}_1(\mathbf{k}, t)$ as a function of nondimensional time $t\omega_c$ at $\mathbf{k} = \mathbf{0}$ for the discrete system (black curves), and the continuum models with $2N = 4$ (red curves) and $2N = 16$ (magenta curves). The curves are perfectly overlapped. (b) Zoom for $t\omega_c \in [0, 10]$.

CRediT authorship contribution statement

Francesca Fantoni: Writing – review & editing, Writing – original draft, Visualization, Methodology, Investigation, Funding acquisition, Formal analysis, Conceptualization. **Andrea Bacigalupo:** Writing – review & editing, Writing – original draft, Visualization, Methodology, Investigation, Funding acquisition, Formal analysis, Conceptualization. **Luigi Gambarotta:** Writing – review & editing, Writing – original draft, Visualization, Methodology, Investigation, Funding acquisition, Formal analysis, Conceptualization.

Declaration of competing interest

The authors declare that they have no known competing financial interests or personal relationships that could have appeared to influence the work reported in this paper.

Data availability

Data will be made available on request.

Acknowledgments

F. Fantoni and A. Bacigalupo are members of INdAM-GNFM. The authors gratefully acknowledge the National Group of Mathematical Physics (GNFM-INdAM, Italy) and the financial support of the European Union – Next Generation EU, under the call PRIN 2022 PNRR of the Italian Minister of University and Research (MUR)-Project P2022HLHHB (PE: Physical Sciences and Engineering): "A digital framework for the cutting of soft tissues: A first step towards virtual surgery".

Funded by the European Union NextGenerationEU

Appendix A. Metamaterial frequency spectrum in terms of Floquet multipliers

In the present Section it is shown how the propagation and the spatial attenuation of waves inside the metamaterial can be tackled in terms of the Floquet multipliers. In the case of non homogeneous waves, namely when the direction of propagation $\mathbf{n}_R$ differs from the direction of attenuation $\mathbf{n}_I$, recalling that the matrix $\mathbf{D}^{(\ell)}(\mathbf{k})$ of the ℓ-th layer has the form $\mathbf{D}^{(\ell)}(\mathbf{k}) = \mathbf{K}^{(\ell)}_{ss} + \sum_{\mathcal{P}_{[j]}} \left[\mathbf{K}^{+(\ell)}_{ss_j} \exp(\imath \mathbf{x}_j \cdot \mathbf{k}) + \mathbf{K}^{-(\ell)}_{ss_j} \exp(\imath \mathbf{x}_j \cdot \mathbf{k})^{-1}\right]$, expressing the vector $\mathbf{x}_j$ in terms of the two lattice's independent periodicity vectors $\mathbf{v}_p$, as $\mathbf{x}_j = a^j_p \mathbf{v}_p = a^j_p v^p_q \mathbf{e}_q$ with $p, q = 1, 2$ and $a^j_p \in \mathbb{Z}^{\leq 1}_{\geq -1}$, the matrix $\mathbf{D}^{(\ell)}(\mathbf{k})$ can be written as

$$\begin{aligned}\mathbf{D}^{(\ell)}(\mathbf{k}) &= \mathbf{K}^{(\ell)}_{ss} + \sum_{\mathcal{P}_{[j]}} \left[\mathbf{K}^{+(\ell)}_{ss_j} \exp\left[\imath\, a^j_p \mathbf{v}_p \cdot \mathbf{k}\right] + \mathbf{K}^{-(\ell)}_{ss_j} \exp\left[-\imath\, a^j_p \mathbf{v}_p \cdot \mathbf{k}\right]\right] = \\ &= \mathbf{K}^{(\ell)}_{ss} + \sum_{\mathcal{P}_{[j]}} \left[\mathbf{K}^{+(\ell)}_{ss_j} \exp\left[\imath\, a^j_p \left(v^p_1 k_1 + v^p_2 k_2\right)\right]\right. \\ &\quad \left. + \mathbf{K}^{-(\ell)}_{ss_j} \exp\left[-\imath\, a^j_p \left(v^p_1 k_1 + v^p_2 k_2\right)\right]\right]. \end{aligned} \tag{52}$$

Introducing the mapping $\lambda_q = \exp(\imath\, l^j_r k_q)$, where λ_q plays the role of a Floquet multiplier with $q = 1, 2$ and l^j_r is a reference length for the lattice at hand, from Eq. (52) the matrix $\mathbf{D}^{(\ell)}(\mathbf{k})$ becomes $\mathbf{D}^{(\ell)}(\lambda_1, \lambda_2)$ with the following expression

$$\mathbf{D}^{(\ell)}(\lambda_1, \lambda_2) = \mathbf{K}^{(\ell)}_{ss} + \sum_{\mathcal{P}_{[j]}} \left[\mathbf{K}^{+(\ell)}_{ss_j} \lambda_1^{a^j_p v^p_1 / l^j_r} \lambda_2^{a^j_p v^p_2 / l^j_r} + \mathbf{K}^{-(\ell)}_{ss_j} \lambda_1^{-a^j_p v^p_1 / l^j_r} \lambda_2^{-a^j_p v^p_2 / l^j_r}\right], \tag{53}$$

and Eq. (5) for the free propagation case (with $\mathring{\mathbf{f}}(\mathbf{k}, s) = \mathbf{0}$) becomes $\mathbf{C}(\lambda_1, \lambda_2, \omega)\mathring{\mathbf{q}}(\lambda_1, \lambda_2, \omega) = \mathbf{0}$, with $\mathbf{C}(\lambda_1, \lambda_2, \omega)$ a polynomial matrix in the complex Floquet multipliers λ_1 and λ_2 with, in general, non integer exponents. Expressing the characteristic polynomial in terms of λ_1, λ_2, and ω, the frequency spectrum is again obtained through the intersection of two hypersurfaces immersed in $\mathbb{R}^5$. Once the Floquet multipliers are

known, in fact, the wave vectors components are simply computed as $k_q = \ln(\lambda_q)/(\imath\, l_r^j)$. Particular cases can be obtained by fixing one of the Floquet multipliers, namely $\lambda_\beta = \exp(\imath\, l_r^j\, k_\beta) = \bar{\lambda}_\beta \in \mathbb{C}$, with $\beta = 1$ or 2, from which

$$\mathbf{D}^{(\ell)}(\lambda_\alpha) = \mathbf{K}_{ss}^{(\ell)} + \sum_{\mathcal{P}_{[j]}} \left[\mathbf{K}_{ss_j}^{+(\ell)} \lambda_\alpha^{a_p^j v_\alpha^p / l_r^j} \bar{\lambda}_\beta^{a_p^j v_\beta^p / l_r^j} + \mathbf{K}_{ss_j}^{-(\ell)} \lambda_\alpha^{-a_p^j v_\alpha^p / l_r^j} \bar{\lambda}_\beta^{-a_p^j v_\beta^p / l_r^j} \right], \tag{54}$$

and the associated eigenproblem simplifies in the form

$$\mathbf{C}(\lambda_\alpha, \omega)\mathring{\mathbf{q}}(\lambda_\alpha, \omega) = \mathbf{0}, \tag{55}$$

with $\alpha = 1$ or 2 and $\alpha \neq \beta$. The corresponding frequency spectrum is thus obtained from the intersection of two hypersurfaces immersed in $\mathbb{R}^3$. If the exponent $a_p^j v_q^p / l_r^j \in \mathbb{Z}$, the matrix $\mathbf{C}(\lambda_\alpha, \omega)$ becomes a polynomial matrix in λ_α with integer exponents and Eq. (55) becomes a polynomial eigenproblem where λ_α is the eigenvalue and $\mathring{\mathbf{q}}(\lambda_\alpha, \omega)$ the eigenvector.

When the wave is homogeneous ($\mathbf{n}_R = \mathbf{n}_I = \mathbf{n}$), fixing the direction $\mathbf{n}$, the matrix $\mathbf{D}^{(\ell)}$ can be expressed in terms of the Floquet multiplier $\lambda_{\mathbf{n}} = \exp(\imath\, k\, l_r)$, with l_r a reference length for the lattice, as

$$\mathbf{D}^{(\ell)}(\lambda_{\mathbf{n}}) = \mathbf{K}_{ss}^{(\ell)} + \sum_{\mathcal{P}_{[j]}} \left[\mathbf{K}_{ss_j}^{+(\ell)} \lambda_{\mathbf{n}}^{a_p^j v_q^p n_q / l_r} + \mathbf{K}_{ss_j}^{-(\ell)} \lambda_{\mathbf{n}}^{-a_p^j v_q^p n_q / l_r} \right]. \tag{56}$$

It still results to be an exponential polynomial in $\lambda_{\mathbf{n}}$ with, generally, non integer exponents, and the frequency spectrum is obtained through the intersection of two hypersurfaces immersed in $\mathbb{R}^3$. In the particular case in which the wave propagation occurs along one of the reciprocal lattice's periodicity directions, the matrix $\mathbf{D}^{(\ell)}(\lambda_{\mathbf{n}})$ can become an exponential polynomial in $\lambda_{\mathbf{n}}$ with integer exponents and the frequency spectrum can be obtained through the resolution of a polynomial eigenproblem where the Floquet multiplier is the eigenvalue. In fact, denoting with $\mathbf{p}_h$, with $h = 1, 2$ the independent periodicity vectors of the reciprocal lattice, they are such that $\mathbf{v}_p \cdot \mathbf{p}_h = 2\pi\delta_{ph}$, with δ_{ph} the Kronecker delta (see Fig. 1). When $\mathbf{n} = \frac{\mathbf{p_h}}{\|\mathbf{p}_h\|_2}$, with h a non summed index, if $l_r = \frac{2\pi}{\|\mathbf{p}_h\|_2}$ the matrix $\mathbf{D}^{(\ell)}(\lambda_{\mathbf{n}\Rightarrow\mathbf{p}_h})$ simplifies into

$$\mathbf{D}^{(\ell)}(\lambda_{\mathbf{n}\Rightarrow\mathbf{p}_h}) = \mathbf{K}_{ss}^{(\ell)} + \sum_{\mathcal{P}_{[j]}} \left[\mathbf{K}_{ss_j}^{+(\ell)} \lambda_{\mathbf{n}\Rightarrow\mathbf{p}_h}^{a_h^j} + \mathbf{K}_{ss_j}^{-(\ell)} \lambda_{\mathbf{n}\Rightarrow\mathbf{p}_h}^{-a_h^j} \right]. \tag{57}$$

If the two independent periodicity vectors $\mathbf{v}_p$ are orthogonal to each other, since $a_h^j \in \mathbb{Z}_{\geq -1}^{\leq 1}$, the eigenproblem $\mathbf{C}(\lambda_{\mathbf{n}\Rightarrow\mathbf{p}_h}, \omega)\mathring{\mathbf{q}}(\lambda_{\mathbf{n}\Rightarrow\mathbf{p}_h}, \omega) = \mathbf{0}$ becomes a quadratic eigenproblem in $\lambda_{\mathbf{n}\Rightarrow\mathbf{p}_h}$. In fact

$$\lambda_{\mathbf{n}\Rightarrow\mathbf{p}_h}\mathbf{D}^{(\ell)}(\lambda_{\mathbf{n}\Rightarrow\mathbf{p}_h}) = \lambda_{\mathbf{n}\Rightarrow\mathbf{p}_h}\mathbf{K}_{ss}^{(\ell)} + \sum_{\mathcal{P}_{[j]}} \left[\mathbf{K}_{ss_j}^{+(\ell)} \lambda_{\mathbf{n}\Rightarrow\mathbf{p}_h}^2 + \mathbf{K}_{ss_j}^{-(\ell)} \right]. \tag{58}$$

Appendix B. Mass and stiffness matrices components for the antitetrachiral topology

In the present Appendix, the non-null components of mass matrices and stiffness-like matrices involved in the dynamics of the undamped antitetrachiral material, as expressed in Eqs. (1), where ligaments have axial stiffness EA/L and flexural one EJ/L^3, are detailed in terms of the geometrical and constitutive parameters. If $u_{\mathcal{J}_1}^{i(\ell)}$ and $u_{\mathcal{J}_2}^{i(\ell)}$ represent the in-plane translational degrees of freedom of the stiff ring i belonging to the $\mathcal{J}$th cell of the ℓth layer, and $\theta_{\mathcal{J}}^{i(\ell)}$ is its rotation with respect to the ring centroid, the twelve by one vector $\mathbf{u}_{\mathcal{J}}^{(\ell)}$ is expressed as

$$\mathbf{u}_{\mathcal{J}}^{(\ell)} = \left(u_{\mathcal{J}_1}^{1(\ell)}\ u_{\mathcal{J}_2}^{1(\ell)}\ \theta_{\mathcal{J}}^{1(\ell)}\ u_{\mathcal{J}_1}^{2(\ell)}\ u_{\mathcal{J}_2}^{2(\ell)}\ \theta_{\mathcal{J}}^{2(\ell)}\ u_{\mathcal{J}_1}^{3(\ell)}\ u_{\mathcal{J}_2}^{3(\ell)}\ \theta_{\mathcal{J}}^{3(\ell)}\ u_{\mathcal{J}_1}^{4(\ell)}\ u_{\mathcal{J}_2}^{4(\ell)}\ \theta_{\mathcal{J}}^{4(\ell)} \right)^T. \tag{59}$$

Analogously, the twelve by one vector $\mathbf{v}_{\mathcal{J}}^{(\ell)}$ reads

$$\mathbf{v}_{\mathcal{J}}^{(\ell)} = \left(v_{\mathcal{J}_1}^{1(\ell)}\ v_{\mathcal{J}_2}^{1(\ell)}\ \phi_{\mathcal{J}}^{1(\ell)}\ v_{\mathcal{J}_1}^{2(\ell)}\ v_{\mathcal{J}_2}^{2(\ell)}\ \phi_{\mathcal{J}}^{2(\ell)}\ v_{\mathcal{J}_1}^{3(\ell)}\ v_{\mathcal{J}_2}^{3(\ell)}\ \phi_{\mathcal{J}}^{3(\ell)}\ v_{\mathcal{J}_1}^{4(\ell)}\ v_{\mathcal{J}_2}^{4(\ell)}\ \phi_{\mathcal{J}}^{4(\ell)} \right)^T, \tag{60}$$

where $v_{\mathcal{J}_1}^{i(\ell)}$ and $v_{\mathcal{J}_2}^{i(\ell)}$ are the in-plane displacements of resonator i belonging to the $\mathcal{J}$th cell of the ℓth layer, while $\phi_{\mathcal{J}}^{i(\ell)}$ is its rotation with respect to the disk centroid. The components of the twelve by twelve stiffness-like matrices involved in the system (1) are denoted as

$$\begin{aligned} &\left[\mathbf{K}_{ss}^{(\ell)}\right]_{ih} = K_{ih}^{ss},\ \left[\mathbf{K}_{ss_j}^{+(\ell)}\right]_{ih} = K_{ih}^{+ss_j},\ \left[\mathbf{K}_{ss_j}^{-(\ell)}\right]_{ih} = K_{ih}^{-ss_j},\\ &\left[\mathbf{K}_{sr}^{(\ell)}\right]_{ih} = \left[\mathbf{K}_{rs}^{(\ell)}\right]_{ih} = K_{ih}^{rs},\ \left[\mathbf{K}_{rr}^{(\ell)}\right]_{ih} = K_{ih}^{rr}. \end{aligned} \tag{61}$$

Without losing generality, their non-null components are made explicit for $\ell = f$ and, for $\mathbf{K}_{ss}^{(\ell)}$ they read

$$\begin{aligned} &K_{11}^{ss} = K_{22}^{ss} = K_{44}^{ss} = K_{55}^{ss} = K_{77}^{ss} = K_{88}^{ss} = K_{10\,10}^{ss} = K_{11\,11}^{ss} = 2\,E\,A/L\\ &\quad + 24\,E\,J/L^3,\\ &K_{33}^{ss} = K_{66}^{ss} = K_{99}^{ss} = K_{12\,12}^{ss} = 16\,E\,J/L + 4E\,A/L\,R^2,\\ &K_{14}^{ss} = K_{41}^{ss} = K_{28}^{ss} = K_{82}^{ss} = K_{5\,11}^{ss} = K_{11\,5}^{ss} = K_{7\,10}^{ss} = K_{10\,7}^{ss} = -E\,A/L,\\ &K_{17}^{ss} = K_{71}^{ss} = K_{25}^{ss} = K_{52}^{ss} = K_{4\,10}^{ss} = K_{10\,4}^{ss} = K_{8\,11}^{ss} = K_{11\,8}^{ss} = -12\,E\,J/L^3,\\ &K_{19}^{ss} = K_{91}^{ss} = K_{35}^{ss} = K_{53}^{ss} = K_{4\,12}^{ss} = K_{12\,4}^{ss} = K_{9\,11}^{ss}\\ &= K_{11\,9}^{ss} = -K_{62}^{ss} = -K_{26}^{ss} = -K_{37}^{ss} = -K_{73}^{ss} = -K_{6\,10}^{ss} =\\ &= -K_{10\,6}^{ss} = -K_{8\,12}^{ss} = -K_{12\,8}^{ss} = -6\,E\,J/L^2,\\ &K_{16}^{ss} = K_{61}^{ss} = K_{29}^{ss} = K_{92}^{ss} = K_{34}^{ss} = K_{43}^{ss} = K_{38}^{ss}\\ &= K_{83}^{ss} = -K_{5\,12}^{ss} = -K_{12\,5}^{ss} = -K_{6\,11}^{ss} = -K_{11\,6}^{ss} = -K_{9\,10}^{ss} =\\ &= -K_{10\,9}^{ss} = -K_{12\,7}^{ss} = -K_{7\,12}^{ss} = E\,A/L\,R,\\ &K_{36}^{ss} = K_{63}^{ss} = K_{39}^{ss} = K_{93}^{ss} = K_{6\,12}^{ss}\\ &= K_{12\,6}^{ss} = K_{9\,12}^{ss} = K_{12\,9}^{ss} = 2\,E\,J/L - E\,A/L\,R^2. \end{aligned} \tag{62}$$

The nonnull components of matrices $\mathbf{K}_{ss_j}^{+(\ell)}$ and $\mathbf{K}_{ss_j}^{-(\ell)}$ are

$$\begin{aligned} &K_{41}^{+ss_1} = K_{10\,7}^{+ss_1} = K_{8\,2}^{+ss_2} = K_{11\,5}^{+ss_2}\\ &= K_{14}^{-ss_1} = K_{7\,10}^{-ss_1} = K_{28}^{-ss_2} = K_{5\,11}^{-ss_2} = -E\,A/L,\\ &K_{43}^{+ss_1} = K_{61}^{+ss_1} = -K_{10\,9}^{+ss_1} = -K_{12\,7}^{+ss_1}\\ &= K_{83}^{+ss_2} = K_{92}^{+ss_2} = -K_{11\,6}^{+ss_2} = -K_{12\,5}^{+ss_2} = K_{16}^{-ss_1} = K_{34}^{-ss_1} =\\ &= -K_{7\,12}^{-ss_1} = -K_{9\,10}^{-ss_1} = K_{29}^{-ss_2} = K_{38}^{-ss_2} = -K_{5\,12}^{-ss_2} = -K_{6\,11}^{-ss_2} = -E\,A/L\,R,\\ &K_{52}^{+ss_1} = K_{11\,8}^{+ss_1} = K_{71}^{+ss_2} = K_{10\,4}^{+ss_2}\\ &= K_{25}^{-ss_1} = K_{8\,11}^{-ss_1} = K_{17}^{-ss_2} = K_{4\,10}^{-ss_2} = -12\,E\,J/L^3,\\ &K_{53}^{+ss_1} = K_{11\,9}^{+ss_1} = -K_{62}^{+ss_1} = -K_{12\,8}^{+ss_1}\\ &= -K_{73}^{+ss_2} = K_{91}^{+ss_2} = -K_{10\,6}^{+ss_2} = K_{12\,4}^{+ss_2} = K_{35}^{-ss_1} = K_{9\,11}^{-ss_1} =\\ &= -K_{26}^{-ss_1} = -K_{8\,12}^{-ss_1} = K_{19}^{-ss_2} = K_{4\,12}^{-ss_2} = -K_{37}^{-ss_2} = -K_{6\,10}^{-ss_2} = 6\,E\,J/L^2,\\ &K_{63}^{+ss_1} = K_{12\,8}^{+ss_j} = K_{93}^{+ss_2} = K_{12\,6}^{+ss_j}\\ &= K_{36}^{-ss_1} = K_{9\,12}^{-ss_1} = K_{39}^{-ss_2} = K_{6\,12}^{-ss_2} = 2\,E\,J/L - E\,A/L\,R^2. \end{aligned} \tag{63}$$

The matrices $\mathbf{K}_{rr}$ and $\mathbf{K}_{rs}$ have the following non null components

$$\begin{aligned} &K_{11}^{rr} = K_{22}^{rr} = K_{44}^{rr} = K_{55}^{rr} = K_{77}^{rr}\\ &= K_{88}^{rr} = K_{10\,10}^{rr} = K_{11\,11}^{rr} = -K_{11}^{rs} = -K_{22}^{rs} = -K_{44}^{rs} = -K_{55}^{rs} =\\ &= -K_{77}^{rs} = -K_{88}^{rs} = -K_{10\,10}^{rs} = -K_{11\,11}^{rs} = \kappa_d,\\ &K_{33}^{rr} = K_{66}^{rr} = K_{99}^{rr} = K_{12\,12}^{rr} = -K_{33}^{rs} = -K_{66}^{rs} = -K_{99}^{rs} = -K_{12\,12}^{rs} = \kappa_\theta, \end{aligned} \tag{64}$$

where, if the resonator is conceived as a rigid mass immersed in a soft matrix inside a rigid ring, the relative ring-resonator translational and rotational stiffnesses κ_d and κ_θ could be simply calibrated as shown, for example, in the Appendix A of Bacigalupo and Gambarotta (2016). Analogously, the components of the twelve by twelve mass matrices of Eqs. (1) are

$$\left[\mathbf{M}_s^{(\ell)}\right]_{ih} = M_{ih}^s,\ \left[\mathbf{M}_r^{(\ell)}\right]_{ih} = M_{ih}^r. \tag{65}$$

The non null components for $\mathbf{M}_s^{(\ell)}$ read

$$\begin{aligned} &M_{11}^s = M_{22}^s = M_{44}^s = M_{55}^s = M_{77}^s = M_{88}^s = M_{10\,10}^s = M_{11\,11}^s = M_s,\\ &M_{33}^s = M_{66}^s = M_{99}^s = M_{12\,12}^s = J_s, \end{aligned} \tag{66}$$

while for $\mathbf{M}_r^{(\ell)}$ they are

$$M^r_{11} = M^r_{22} = M^r_{44} = M^r_{55} = M^r_{77} = M^r_{88} = M^r_{10\,10} = M^r_{11\,11} = M_r,$$
$$M^r_{33} = M^r_{66} = M^r_{99} = M^r_{12\,12} = J_r. \tag{67}$$

References

Aifantis, K., Willis, J., 2006. Scale effects induced by strain-gradient plasticity and interfacial resistance in periodic and randomly heterogeneous media. Mech. Mater. 38 (8–10), 702–716.

Alderson, A., Alderson, K., 2007. Auxetic materials. Proc. Inst. Mech. Eng. G 221 (4), 565–575.

Andrianov, I.V., Starushenko, G.A., Weichert, D., 2012. Numerical investigation of 1D continuum dynamical models of discrete chain. ZAMM-J. Appl. Math. Mech./Z. Angew. Math. Mech. 92 (11–12), 945–954.

Askes, H., Aifantis, E.C., 2011. Gradient elasticity in statics and dynamics: an overview of formulations, length scale identification procedures, finite element implementations and new results. Int. J. Solids Struct. 48 (13), 1962–1990.

Askes, H., Metrikine, A.V., 2005. Higher-order continua derived from discrete media: continualisation aspects and boundary conditions. Int. J. Solids Struct. 42 (1), 187–202.

Askes, H., Suiker, A., Sluys, L., 2002. A classification of higher-order strain-gradient models–linear analysis. Arch. Appl. Mech. 72 (2–3), 171–188.

Bacigalupo, A., Gambarotta, L., 2016. Simplified modelling of chiral lattice materials with local resonators. Int. J. Solids Struct. 83, 126–141.

Bacigalupo, A., Gambarotta, L., 2017a. Dispersive wave propagation in two-dimensional rigid periodic blocky materials with elastic interfaces. J. Mech. Phys. Solids 102, 165–186.

Bacigalupo, A., Gambarotta, L., 2017b. Wave propagation in non-centrosymmetric beam-lattices with lumped masses: discrete and micropolar modeling. Int. J. Solids Struct. 118, 128–145.

Bacigalupo, A., Gambarotta, L., 2019. Generalized micropolar continualization of 1D beam lattices. Int. J. Mech. Sci. 155, 554–570.

Bacigalupo, A., Gambarotta, L., 2021. Identification of non-local continua for lattice-like materials. Internat. J. Engrg. Sci. 159, 103430.

Bacigalupo, A., Lepidi, M., 2016. High-frequency parametric approximation of the Floquet-Bloch spectrum for anti-tetrachiral materials. Int. J. Solids Struct. 97, 575–592.

Beex, L., Peerlings, R., Geers, M., 2014. A multiscale quasicontinuum method for dissipative lattice models and discrete networks. J. Mech. Phys. Solids 64, 154–169.

Casolo, S., 2021. A linear-elastic heuristic-molecular modelling for plane isotropic micropolar and auxetic materials. Int. J. Solids Struct. 224, 111042.

Challamel, N., Aydogdu, M., Elishakoff, I., 2018. Statics and dynamics of nanorods embedded in an elastic medium: Nonlocal elasticity and lattice formulations. Eur. J. Mech. A Solids 67, 254–271.

Challamel, N., Kocsis, A., Wang, C., 2015. Discrete and non-local elastica. Int. J. Non-Linear Mech. 77, 128–140.

Chang, C.S., Gao, J., 1995. Second-gradient constitutive theory for granular material with random packing structure. Int. J. Solids Struct. 32 (16), 2279–2293.

Charlotte, M., Truskinovsky, L., 2012. Lattice dynamics from a continuum viewpoint. J. Mech. Phys. Solids 60 (8), 1508–1544.

Colquitt, D., Jones, I., Movchan, N., Movchan, A., 2011. Dispersion and localization of elastic waves in materials with microstructure. Proc. R. Soc. A: Math. Phys. Eng. Sci. 467 (2134), 2874–2895.

Deshpande, V.S., Fleck, N.A., Ashby, M.F., 2001. Effective properties of the octet-truss lattice material. J. Mech. Phys. Solids 49 (8), 1747–1769.

Diana, V., Bacigalupo, A., Gambarotta, L., 2023. Thermodinamically-consistent dynamic continualization of block-lattice materials. Int. J. Solids Struct. 262, 112050.

Dirrenberger, J., Forest, S., Jeulin, D., 2013. Effective elastic properties of auxetic microstructures: anisotropy and structural applications. Int. J. Mech. Mater. Des. 9, 21–33.

Evans, K.E., Alderson, A., 2000. Auxetic materials: functional materials and structures from lateral thinking!. Adv. Mater. 12 (9), 617–628.

Fantoni, F., Bacigalupo, A., 2020. Wave propagation modeling in periodic elasto-thermo-diffusive materials via multifield asymptotic homogenization. Int. J. Solids Struct. 196–197, 99–128.

Fantoni, F., Bacigalupo, A., Gnecco, G., Gambarotta, L., 2023. Multi-objective optimal design of mechanical metafilters based on principal component analysis. Int. J. Mech. Sci. 248, 108195.

Fleck, N.A., Deshpande, V.S., Ashby, M.F., 2010. Micro-architectured materials: past, present and future. Proc. R. Soc. A: Math. Phys. Eng. Sci. 466 (2121), 2495–2516.

Forest, S., Sab, K., 1998. Cosserat overall modeling of heterogeneous materials. Mech. Res. Commun. 25 (4), 449–454.

Greaves, G.N., Greer, A.L., Lakes, R.S., Rouxel, T., 2011. Poisson's ratio and modern materials. Nat. Mater. 10 (11), 823–837.

Greer, J.R., Deshpande, V.S., 2019. Three-dimensional architected materials and structures: Design, fabrication, and mechanical behavior. MRS Bull. 44 (10), 750–757.

Hache, F., Challamel, N., Elishakoff, I., Wang, C., 2017. Comparison of nonlocal continualization schemes for lattice beams and plates. Arch. Appl. Mech. 87, 1105–1138.

Hörmander, L., 2007. Pseudo-differential operators. The Analysis of Linear Partial Differential Operators III: Pseudo-Differential Operators 63–179.

Jia, Z., Yu, Y., Hou, S., Wang, L., 2019. Biomimetic architected materials with improved dynamic performance. J. Mech. Phys. Solids 125, 178–197.

Jordán, K., 1965. Calculus of Finite Differences. vol. 33, American Mathematical Soc..

Kohn, J., 1973. Pseudo-differential operators and hypoellipticity. Part. Differ. Equ. 23, 61.

Kumar, R.S., McDowell, D.L., 2004. Generalized continuum modeling of 2-D periodic cellular solids. Int. J. Solids Struct. 41 (26), 7399–7422.

Kunin, I.A., 2012. Elastic Media with Microstructure I: One-Dimensional Models. vol. 26, Springer Science & Business Media.

Lakes, R., 1991. Deformation mechanisms in negative Poisson's ratio materials: structural aspects. J. Mater. Sci. 26, 2287–2292.

Liu, J., Chen, X., Xu, L.X., 1999. New thermal wave aspects on burn evaluation of skin subjected to instantaneous heating. IEEE Trans. Biomed. Eng. 46 (4), 420–428.

Liu, A., Zhu, R., Liu, X., Hu, G., Huang, G., 2012. Multi-displacement microstructure continuum modeling of anisotropic elastic metamaterials. Wave Motion 49 (3), 411–426.

Madeo, A., Neff, P., Ghiba, I.-D., Placidi, L., Rosi, G., 2015. Wave propagation in relaxed micromorphic continua: modeling metamaterials with frequency band-gaps. Contin. Mech. Thermodyn. 27, 551–570.

Mindlin, R.D., 1964. Micro-structure in linear elasticity. Arch. Ration. Mech. Anal. 16, 51–78.

Mühlhaus, H., Oka, F., 1996. Dispersion and wave propagation in discrete and continuous models for granular materials. Int. J. Solids Struct. 33 (19), 2841–2858.

Nannapaneni, R.G., Nakshatrala, K.B., Stefaniuk, D., Krakowiak, K.J., 2021. Discrete lattice modeling of wave propagation in materials with heterogeneous microstructures. J. Eng. Mech. 147 (10), 04021075.

Ostoja-Starzewski, M., 2002. Lattice models in micromechanics. Appl. Mech. Rev. 55 (1), 35–60.

Pham, M.-S., Liu, C., Todd, I., Lertthanasarn, J., 2019. Damage-tolerant architected materials inspired by crystal microstructure. Nature 565 (7739), 305–311.

Prawoto, Y., 2012. Seeing auxetic materials from the mechanics point of view: A structural review on the negative Poisson's ratio. Comput. Mater. Sci. 58, 140–153.

Romijn, N.E., Fleck, N.A., 2007. The fracture toughness of planar lattices: Imperfection sensitivity. J. Mech. Phys. Solids 55 (12), 2538–2564.

Rosenau, P., 2003. Hamiltonian dynamics of dense chains and lattices: or how to correct the continuum. Phys. Lett. A 311 (1), 39–52.

Rota, G.-C., 1964. On the foundations of combinatorial theory: I. Theory of Möbius functions. In: Classic Papers in Combinatorics. Springer, pp. 332–360.

Rubin, M., Rosenau, P., Gottlieb, O., 1995. Continuum model of dispersion caused by an inherent material characteristic length. J. Appl. Phys. 77 (8), 4054–4063.

Schaedler, T.A., Carter, W.B., 2016. Architected cellular materials. Annu. Rev. Mater. Res. 46, 187–210.

Schraad, M.W., Triantafyllidis, N., 1997a. Scale effects in media with periodic and nearly periodic microstructures, Part I: Macroscopic properties. ASME. J. Appl. Mech. 64, 751–762.

Schraad, M., Triantafyllidis, N., 1997b. Scale effects in media with periodic and nearly periodic microstructures, Part II: failure mechanisms. ASME. J. Appl. Mech. 64, 763–771.

Trovalusci, P., Masiani, R., 1999. Material symmetries of micropolar continua equivalent to lattices. Int. J. Solids Struct. 36 (14), 2091–2108.

Vigliotti, A., Deshpande, V.S., Pasini, D., 2014. Non linear constitutive models for lattice materials. J. Mech. Phys. Solids 64, 44–60.

Wadley, H.N., Fleck, N.A., Evans, A.G., 2003. Fabrication and structural performance of periodic cellular metal sandwich structures. Compos. Sci. Technol. 63 (16), 2331–2343.

Xia, X., Afshar, A., Yang, H., Portela, C.M., Kochmann, D.M., Di Leo, C.V., Greer, J.R., 2019. Electrochemically reconfigurable architected materials. Nature 573 (7773), 205–213.

Zhang, Z., Wang, C., Challamel, N., Elishakoff, I., 2014. Obtaining Eringen's length scale coefficient for vibrating nonlocal beams via continualization method. J. Sound Vib. 333 (20), 4977–4990.